HEAT TRANSFER MEASUREMENTS IN PARTIALLY IONIZED GASES

by

P. H. Rose and J. O. Stankevics

AVCO-EVERETT RESEARCH LABORATORY
a division of
AVCO CORPORATION
Everett, Massachusetts

July 1964

Contract No. NAS w-748

prepared for

HEADQUARTERS
NATIONAL AERONAUTICS AND SPACE ADMINISTRATION
OFFICE OF ADVANCED RESEARCH AND TECHNOLOGY
Washington 25, D. C.

ABSTRACT

27315

Over the past few years a number of theoretical and experimental investigations have been published on the subject of convective energy transport in a high temperature partially ionized gas. Although, in general a fair degree of understanding of this process is now available, certain uncertainties have arisen, particularly with respect to the effect of the surface material of the heat transfer gage. This experimental investigation brings a new technique of making heat transfer measurements to bear on this problem.

The infrared heat transfer gage developed by Camac has been adapted to the problems peculiar to this experiment. An analysis is presented which demonstrates the response required of the measurement in order to enable accurate heat transfer measurements to be made within the limited test times available. The difficulties of adapting the gage to the requirements are described, in particular the sensitivity, opacity, and adherence of the gage to the MgO window. The calibration of the absolute magnitude of the output of the infrared cell as well as the response time of the measuring system are described in detail. The response of the gage to the heat transfer encountered in both the shock tube end wall and on a model are discussed with emphasis on the identification of radiative heat transfer effects.

The heat transfer results support the previous results of the authors with calorimeter gages as well as those of other investigations. Variations of the gage surface material achieved by overcoating the carbon with thin metallic films did not change the heat transfer rates measured, in contrast to the results reported by Warren. In view of the fact that the metallic films used do not change the calibration of the gage this is felt to be a conclusive result regarding the effect of surface materials.

Author

TABLE OF CONTENTS

SECTION I

INTRODUCTION

Accurate definition of the severity of the planetary entry problem has been made difficult by the complexity of performing experiments in this environment. Although several experimental studies[1,2,3] have indicated a general agreement of their measurements with the theoretical work of Fay and Kemp,[4] Pallone,[5] and Hoshizaki,[6] it has been pointed out that all these measurements depended on a common technique, the platinum, calorimeter, or thick film resistance thermometer. Experiments by Warren and Gruszczynski[7] have indicated that results of considerable variance can be obtained by the simple expediency of changing the gage material of the calorimeter.

In this situation it was felt that a completely independent measurement of convective heat transfer by a different experimental technique would be worthwhile in settling the uncertainties which have been raised by the above experimental facts. The infrared heat transfer gage developed by Camac[8] appeared to be available to make this independent judgment. Not only does this gage measure heat transfer through a completely different sensor system, but it also had the added advantage of being able to assess the effects of surface materials without a change in the calibration of the instrument. This, of course, could be accomplished by coating the same carbon infrared emitting surface with metallic coatings of various elements, and yet not change the infrared emission characteristics of the carbon.

This paper reports on an experiment in which the infrared heat transfer gage was adapted to measure the stagnation point heat transfer on the spherical nose of a model. The experiments were performed in a six-inch I.D. arc-heated driver shock tube thoroughly discussed in the literature.[9] The existence of a homogeneous hot gas sample of predictable conditions in this shock tube has been documented in Refs. 1 and 9. In the present experiments the tube was used at a length of 30 feet and an initial pressure of 0.25 mm Hg of air.

The principle of the infrared heat transfer gage has been discussed in detail by Camac.[8] In its simplest form, the gage consists of a thin, but opaque, surface of carbon deposited in good thermal contact on an infrared transmitting window. The carbon surface is exposed to the heat transfer medium while the rear surface of this layer is viewed through the window with a wide angle optical system which is imaged on the infrared detector. The obvious advantage of this gage is that it is electrically decoupled from the gas and consequently there is no mechanism by which the ionized gases can interfere with the gage output.

The purpose of the present experiment was to combine these two techniques to provide the confirmation of the previous work on convective heat transfer. This combination has required the solution of a number of problems, such as gage sensitivity, gage opacity, gage response, analysis of the data taken in times only somewhat longer than the gage response, and system calibration. The approaches and solutions found to these problems as well as the results will be discussed briefly in the following sections.

SECTION II

ANALYSIS OF GAGE RESPONSE

The temperature response of an infinite slab to an ideal heat transfer pulse has been thoroughly covered in the literature;[10] a constant heat transfer rate gives the familiar rise of surface temperature varying with the square root of time, and a heat transfer rate decaying as $1/\sqrt{t}$ gives the familiar jump to a constant temperature. The infrared heat transfer gage response to such an ideal heat transfer pulse has been treated by Camac.[8] The problem is made more complex by the fact that the infrared detector is imaged on the rear surface of the carbon layer.

Two factors complicate the analysis still further; one, the gage system also has a finite response time which with extreme care can be kept to about one microsecond, and second, the heat pulse imposed on the element is an odd combination of ideal pulses, i.e., one that decays inversely with the square root of time as the shock is reflected off the nose of the model and approaches the steady state geometry and the second a constant heat transfer rate pulse after the flow geometry has been established.

The interrelation of these three effects and their relationship to achieving accurate heat transfer measurements within the test time available has been investigated in some detail. Following Camac, for an arbitrary heat transfer rate time history, $\dot{q}(t)$, the convolution theorem gives the temperature response at the interface of a composite surface, i.e., at $x = 0$, as

$$T(t, x=0) = \int_0^t \dot{q}(t') T_\delta(t-t') \, dt' \qquad (1)$$

where $T_\delta(t')$ is the temperature response to a δ function heat input at time

$t = t'$. This temperature response can be written as

$$T_\delta(t, x=0) = \frac{1}{\sqrt{\pi k_1 \rho_1 C_1 t}} \cdot \frac{2}{1+\sigma} \sum_{n=0}^{\infty} \left(\frac{1-\sigma}{1+\sigma}\right)^n e^{-(2m+1)^2 \ell^2 \frac{\rho_1 C_1}{4 k_1 t}} \qquad (2)$$

Combining Eqs. (1) and (2),

$$T(t, x=0) = \frac{2\sigma}{1+\sigma} \frac{1}{\sqrt{\pi k_2 \rho_2 C_2}} \int_0^t \frac{\dot{q}(t')}{\sqrt{t-t'}} \sum_{n=0}^{\infty} \left(\frac{1-\sigma}{1+\sigma}\right)^n e^{-(2m+1)^2 \frac{\tau_1}{t-t'}} dt' \qquad (3)$$

$$\text{where: } \tau_1 \equiv \frac{\ell^2 \rho_1 C_1}{4 k_1}$$

For the case of the heat transfer rate decaying inversely with the square root of time, i.e., $\dot{q} = \frac{Q}{\sqrt{t}}$, Eq. (3) can be shown to be numerically equal to the result used by Camac to show the effect of the thermal lag of the carbon layer, i.e.,

$$T(t, x=0) = \frac{2}{1+\sigma} \sum_{n=0}^{\infty} \left(\frac{1-\sigma}{1+\sigma}\right)^n \frac{Q\pi}{\sqrt{\pi k_1 \rho_1 C_1}} \, \text{erfc} \sqrt{\frac{(2n+1)^2 \ell^2 \rho_1 C_1}{4 k_1 t}} \qquad (4)$$

The second effect which must be considered is that although the temperature response of the interface is the desired quantity, the actual infrared gage output as indicated on the oscilloscope, lags behind this quantity by the finite time response of the gage amplifier oscilloscope circuit. If we replace all the circuit elements by a capacitance and resistance in the simple circuit shown below
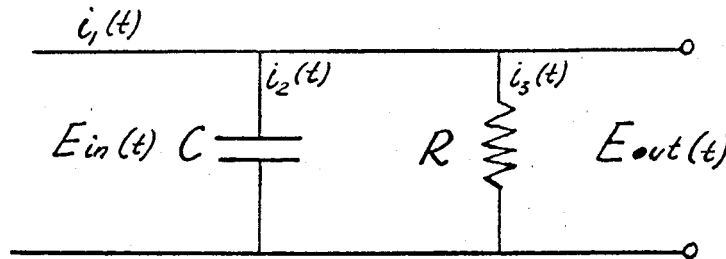
then the problem is reduced to finding the accuracy with which $E_{out}(t)$ responds to its input $E_{in}(t)$. It can be shown that the current in the resistor R can be written as

$$i_3(t) = e^{-t/\tau_2} \int_0^t i_1(t') e^{t'/\tau_2} \frac{dt'}{\tau_2} \qquad (5)$$

-4-

where $\tau_2 = RC$. If we assume that we are operating in a linear region of the gage output curve, i.e., $T \alpha E$, which is only true approximately and over a limited temperature range, then the above can be written as

$$T_{out}(t) = e^{-t/\tau_2} \int_0^t T_{in}(t') e^{t/\tau_2} \frac{dt'}{\tau_2}$$ (6)

Thus, even though the input to the IR gage were perfect, i.e., $T_{in}(t)$, the output would be degraded by the time constant of the system, τ_2.

The third effect is due to the complex heat pulse imposed on the model. When the incident shock arrives at the model, it reflects initially as it would off a solid end wall. The initial reflected shock velocity is known from the Rankine-Hugoniot equations, i.e., Ref. 11. At a shock velocity of 8 mm/μsec and an initial pressure of 0.25 mm of Hg, the reflected shock will start at a velocity of 1.11 mm/μsec and would thus have a characteristic e-folding time to achieve its steady state location of approximately $\epsilon R_s/1.11$, where ϵ is the density ratio across the shock and R_s is the radius of the bow shock in its permanent geometry. For a body with a nose radius of 1.905 cm this time would be almost 3 μsec.

During these three microseconds the heat transfer to the body would be essentially that characteristic of an end wall of a shock tube, i.e., a rate decaying inversely with the square root of time. This is the behavior of heat transfer through a thermal boundary layer growing with time. At some time the three-dimensional effects will become dominant, and the viscous boundary layer will form to its steady geometry. This time has been estimated to be roughly the time required for a sound wave to reach the sonic point; which can be approximated by the nose radius divided by the stagnation sound speed. For the above conditions, this amounts to 6 to 7 microseconds. Such times are in agreement with the times estimated for the calorimeter heat transfer gage output to reach a steady value.[1] Thus, a time of the order of five microseconds is taken up by this process of setting up the steady flow geometry.

It is possible to estimate the expected heat transfer rates during this transient period. As the simplest approximation we assume that the

reflected shock flow geometry applies until the heat transfer drops below the steady state, bow shock geometry value at which time we take the constant heat transfer solution to apply. For the end wall geometry the heat transfer can be written as,[12]

$$\dot{q}_e \sqrt{t} = 0.88 \sqrt{\frac{k_w \rho_w}{c_{p_w}}} \left(h_e - h_w\right) \left(\frac{N_u}{\sqrt{R_e}}\right)' \tag{7}$$

where $(N_u/\sqrt{R_e})'$ is the value of $N_u/\sqrt{R_e}$ evaluated at the same stagnation pressure and enthalpy from stagnation point boundary layer calculations.[4] For the boundary layer case the equivalent expression is

$$\dot{q}_s \sqrt{R} = \frac{1}{\sigma_w^{1/2}} \sqrt{\frac{k_w \rho_w}{c_{p_w}}} \left(\frac{2 p_s}{\rho_s}\right)^{1/4} \frac{N_u}{\sqrt{R_e}} \left(h_s - h_w\right) \tag{8}$$

It can be seen that the two expressions are almost identical except for the nose radius effect in the stagnation point case, which manifests itself in the stagnation point velocity gradient term, $\frac{1}{R} \sqrt{2 \, p_s/\rho_s}$. The ratio of these two expressions gives a clue to which is the dominant one, i.e.,

$$\frac{\dot{q}_e}{\dot{q}_s} = \frac{\sigma_w^{1/2} \, 0.88 \left(N_u/\sqrt{R_e}\right)'}{\sqrt{\frac{t}{R}} \left(\frac{2 p_s}{\rho_s}\right)^{1/4} \left(N_u/\sqrt{R_e}\right)} \tag{9}$$

For the typical conditions of this experiment, the above ratio is very close to unity at times of approximately one microsecond, varying with t and R as indicated. The ratio of the Nusselts numbers is essentially one, as the pressure and enthalpy do not vary greatly between stagnation and reflected conditions. The values of q_e and q_s are plotted in Fig. 1 for the specific case of $p_1 = 0.25$ mm of Hg, $U_s = 8$ mm/μsec and $R_N = 1.905$ cm. At one microsecond q_e is 1.91 times q_s while at about 3.6 μsec the two are equal. For smaller bodies q_s would increase with $1/\sqrt{R_N}$ and consequently the two would be equal earlier.

In order to determine the requirements on the I. R. gage system to accurately reproduce the heating rates within the limit of test times available, in terms of the lag times due to the carbon layer, as well as the circuitry, numerical experiments were performed. Using the heat transfer time history shown in Fig. 1, we determined the temperature response of the window-carbon interface from Eq. (3) for various values of τ_1. This result can then be used as $T_{in}(t)$ in order to evaluate the effect of finite circuit response by use of Eq. (6) with various values of τ_2. The resulting $T_{out}(t)$ is representative of the signals which are interpreted as the response of the gage to the heating in the actual experiments.

The final step in the numerical experiment is to subject the $T_{out}(t)$ in the usual manner for reduction of transient heat transfer data. This is accomplished by solution of the inverted form of the heat conduction equation (13), i.e.,

$$\dot{q}(t) = \sqrt{\frac{k_2 \rho_2 C_2}{\pi}} \left[\frac{T(t)}{\sqrt{t}} + \frac{1}{2} \int_0^t \frac{T(t) - T(t')}{\sqrt{(t - t')^3}} \, dt' \right] \tag{10}$$

The resulting plots of heat transfer rate, $\dot{q}$ vs time, give the degree to which the input data have been degraded due to various values of τ_1 and τ_2. A set of such results, are shown in Figs. 2 and 3. It was concluded from these results that values of $\tau_1 \leq 10^{-7}$ and $\tau_2 \leq 2 \times 10^{-6}$ seconds were tolerable under the experimental conditions. Figure 4 shows an example of the $T_{out}(t)$ history which is the temperature history expected in the experiments. The plot is made for the values of τ_1 and τ_2 typical for the present experiments, 10^{-7} and 10^{-6} secs respectively.

This judgment is of course strongly tempered by the test times available in the experiment. If the transient phase consumes approximately 5 μsec and the lags of the measurements are such as to spread this time into 10 μsec, it will be very marginal to make meaningful experiments in test times much less than 20 μsec. The performance of the shock tube used with respect to achievement of a uniform test gas has been discussed in Ref. 9 and is reasonably predictable from the work of Roshko.[14] At the conditions of the present experiments average test times of 15 μ sec are

common. Thus the one to two microsecond criteria for the response of the gage system appeared critical.

If the resolution function of any given instrument is know a priori then the measurement can of course be corrected after the fact for the degradation of information due to this resolution. For the case of the circuit response as shown in Eq. (6), this is a reasonable procedure and can be used to lessen the criteria on the electronics. Equation (6) can be inverted by use of LaPlace transforms into a form where $T_{in}(t)$ can be expressed in terms of the measured $T_{out}(t)$ and the time constant of circuit, τ_2, giving

$$T_{in}(t) = T_{out}(t) + \tau_2 \frac{dT_{out}}{dt} \tag{11}$$

Equation (11) can thus be used to recover the original signal with some degree of accuracy.

The above discussion of the difficulties of making accurate temperature measurements which in turn accurately reflect the heat transfer imposed on the surface is extremely important for shock tube experiments in which the test times are very limited. For the model experiments in the high velocity range, the average test times are only two to four times as long as the time required to set up the equilibrium flow geometry. As a consequence, it is clear from these calculations that the response must be kept very fast, and that response times of the order of one microsecond are required.

SECTION III

EXPERIMENTAL TECHNIQUES AND INSTRUMENTATION

Adaptation of the infrared heat transfer gage technique to the present experiments has involved the solution of several unique problems; such as gage opacity, sensitivity, thermal adherence in the environment, dynamic calibration, and dynamic measurement of the gage response.

The opacity requirement can be seen from the following simple considerations. The stagnation point gases are of the order of 10 - 15,000°K. The contribution from this gas in the wavelength range of 1 to 10μ is between 10^3 and 10^4 times as great as the signal from the carbon temperature rise which is being measured. Thus opacity means rejection of one part in 10^4 or better still 10^5. It was not possible to achieve this degree of opacity with only a carbon layer and yet maintain this layer thin enough to meet the response requirements. The addition of a metallic layer allowed fulfillment of the opacity requirement, while maintaining the fast response needed. Final opacity checks were performed by exposing the coated window element to a very intense light source (Lyman Lamp) and measuring the attenuation due to the window and its coatings.

The sensitivity of the gage was optimized by the choice of window material, detector and optical system. As a window material, magnesium oxide was chosen due to its optical characteristics. The radiation from the carbon layer which heats up to a maximum of 150°C during the experiment is predominantly in the 4 to 30 micron wavelength band. The Philco GPC 201 gold-doped germanium infrared detector cuts off at about nine microns. The combination of this detector and window allows almost optimum transmission at wavelengths up to the capability of the detector.

Figure 5 shows the external transmission characteristics of

magnesium oxide crystals (MgO 0.50 mm thick) as used in this experiment measured with a Beckman DK-2 and a Perkin-Elmer infrared spectrophotometer. The transmission is about 86 percent from 0.7 to 7 microns; it then decreases to zero at about 11 microns but is level at about 80 percent from 0.7 to 0.35 microns, then decreasing to zero at about 0.2 microns. MgO crystals show both good mechanical strength as well as infrared transparency at elevated temperatures up to $1000^{\circ}C$.[15] A number of MgO crystals have been checked for external transmission at room temperature after repeated heating to elevated temperatures during the process of depositing carbon layers with a variance of only one percent.

The fused MgO crystals, supplied by Norton Company, were so-called "Magnorite" which have the following properties pertinent to this experiment:

$$\begin{array}{lll} \text{Density} \quad \rho & = 3.576 \ \ \text{gm/cc at } 25^{\circ}C \\ \text{Thermal Conductivity} \ \ k & = 0.0775 \ \text{cal/sec-cm-}^{\circ}C \ \text{at } 20\text{-}100^{\circ}C \\ \text{Specific Heat} \ \ C & = 0.245 \ \text{cal/gm - }^{\circ}C \ \text{at } 20\text{-}200^{\circ}C \end{array}$$

The infrared detector used in these experiments was the Philco GPC-201, a photo conductive, P type, gold-doped germanium detector designed for operation at liquid nitrogen temperatures. The GPC 201 package design has a 2 mm square cell element and a coated silicon window, all enclosed in a strong, hermetically-sealed unit utilizing fuzed glass to metal seals. Typical characteristics of this cell at $T = 77^{\circ}K$ are:

$$\begin{array}{ll} D^{*} \ (500, \ 900, \ 1): & 2.9 \times 10^{9} \ \text{cm/watt} \\ \text{Optimum Bias Voltage:} & 40 \ \text{volts} \\ \text{Time Constant:} & 0.5 - 1.0 \times 10^{-6} \ \text{sec} \end{array}$$

where D^{*} is defined as the square root of the cell area (in cm^{2}) divided by the Noise Equivalent Power. Figure 6 shows the spectral responsivity of the infrared cell used in these experiments.

The optical system built into the model and test section is shown in Figs. 7 and 8. The sensitivity is optimized by the use of a Cassegrain mirror arrangement, as suggested by Camac. By maintaining a

spherical nose past the sonic point (approximately 40°), a larger diameter mirror could be used to enhance the solid angle of the collector system. In some experiments a phototube operating in the visible wavelength region monitored the light in the mirror system for evidence of transmitted light.

The deposition of sufficiently uniform, thin and adhering carbon layers on the MgO crystals was by chemical decomposition (pyrolysis) of methyl iodide, CH_3I, as suggested by Camac.[8] MgO windows, 0.50 mm thick, were roughened on one side with "Norbide" #280 grit, to a surface roughness of about 1/2 micron. On polished MgO crystals, carbon coatings would invariably peel off. The clean, roughened, MgO window was then placed on a platinum strip, rough side up, into a vacuum bell jar containing a mixture of methyl iodide and helium. The platinum and MgO windows were heated in this atmosphere, and the CH_3I decomposes on contact with the hot surfaces. As an end product of this decomposition we achieve a strong black layer of pyrolytic graphite on the MgO substrate. A thickness of about 4000 - 8000 Å is deposited in approximately 15 minutes, which is opaque and measures to have optical densities between 5 and 8. (A unit of optical density is a factor of 10 in the transmission measured at visible wavelengths.)

This method of deposition is assumed to produce pyrolytic graphite. The high degree of anisotropy in the structure of pyrolytic graphite results in thermal properties, other than specific heat, which are considerably different from commercial graphite. In calculating the response of the rear face of the carbon layer, as discussed in the previous section, the properties of pyrolytic graphite were used as reported in Ref. 16. These are:

Density ρ		= 2.22	gm/cc
Thermal Conductivity k		= .0048	cal/sec-cm-°C at 50-150°C
Specific Heat C_p		= .16	cal/gm -°C at 50 - 150°C

Overcoating the carbon layer with a metallic reflecting layer increases the thermal lag of the composite structure, increases the opacity and changes the absorption characteristics of the surface. The latter has the effect of allowing convective heat transfer measurements

-11-

to be made in a radiating gas because most of the incident radiation can be reflected. The metallic layers, which were about 1000-5000 Å thick, were vacuum coated onto the carbon sublayers. This thickness of metal has a characteristic thermal diffusion time an order of magnitude less than the carbon, and thus the thermal response was not significantly affected. Uniform deposition of metallic films (aluminum, gold, copper, Nichrome) was obtained by following Refs. 17 and 18. The coatings were obtained by using hot multistrand helical tungsten filaments and room-temperature coated MgO windows, all in a vacuum of 0.4×10^{-4} to 10^{-4} mm of Hg. Each coating was checked both visually under a microscope as well as in a dark room with the high intensity light source.

The surface of these coatings exhibited the characteristics of the carbon layers and appeared diffuse in reflectance. Since quantitative work on the adherence of evaporated metal films on pyrolytic graphite is not available in the literature, we concluded from visual evidence that chemically reactive metals, such as aluminum, which normally adhere very well to glass,[17,18] and other clean, non-oily inorganic substrates, also adhere to the carbon layer.

For calculations of the thermal lag and heat capacity effects due to the metal films, the bulk properties of the pure metal were used. However, it is known that the properties, particularly the strength, of thin films can vary significantly from the bulk properties.[18]

SECTION IV

CALIBRATION OF THE INFRARED GAGE SYSTEM

The calibration of the infrared heat transfer gage system consists of calibration of the absolute value of the output as well as the response. The former followed closely the procedure outlined by Camac[8] of replacing the shock tube heat source by a black body heat source. A standard black body source was constructed in which a black body cavity was heated by well agitated silicon oil through the temperature range of 0°C to 190°C. The cavity temperature was read by a number of thermocouples distributed to check the uniformity of the cavity. The set-up for the calibration is shown in Fig. 9. A beam chopper placed in front of the black body source provides the AC method chopping at a frequency of 5000/sec. The emission of the chopper blade serves as the reference level as it is seen by the detector when the system is "closed." The output of the cell is fed through a standard cathode follower to an amplifier whose output is displayed on the oscilloscope.

In the shock tube experiment, the heat transfer gage senses a heating pulse of only 15 to 30 μ sec duration. The temperature of the opaque layers rises up to 150°C during this time but the MgO window remains essentially at room temperature. The calibration of the detector output for these short pulses can be evaluated by a series of four hypothetical measurements, as suggested by Reference 8. Figure 10 shows the results of the two actual measurements required by this calibration procedure in terms of the infrared detector output plotted as a function of the temperature of the black body source. The highest output of the infrared cell, V_1, occurs when the black body source is imaged directly on the detector. Here,

$$V_1 = V_B - V_C \tag{12}$$

where V_B is the voltage output due to the black body source and V_C is
the signal due to the temperature of the chopper wheel. V_C is also the
signal from the black body when it is at the same temperatures as the
chopper blade.

The lowest output curve in Fig. 10 is generated by the addition
of the MgO windows to the holes in the chopper wheel. These windows
degrade the transmission by the external transmission loss, X, averaged
over the spectral sensitivity of the gold-doped germanium detector.
These windows are, of course, at the chopper wheel temperature which
is essentially room temperature. This output, V_2 is essentially

$$V_2 = X(V_B - V_C) \tag{13}$$

where the external transmission coefficient, X, is the result of combin-
ing the reflectivity at the two air-MgO interfaces, r, and the internal
absorption of the MgO, a, as follows

$$X = (1 - r)^2 e^{-\alpha x} \tag{14}$$

A third output can be generated if the MgO window is allowed to
come to the temperature of the black body source and thus the output of
the detector will be V_1 degraded only by one single reflection loss at
the MgO-air interface.

$$V_3 = (1 - r)V_B - V_C = V_1(1 - r) \tag{15}$$

A fourth output can be generated if the MgO window is coated by
an opaque carbon layer, and the whole unit is maintained at the temper-
ature of the black body source. The detector output can now be written
as

$$V_4 = \left[\left(\frac{\epsilon X}{1 - r} \right) + \left(1 - r + \frac{X}{1 - r} \right) \right] (V_B - V_C) \tag{16}$$

where ϵ is the emissivity of the carbon-magnesium oxide interface.

-14-

Values of r of 0.065 $\pm$ .005 have been measured for MgO.

The first term in Eq. (16) represents the contribution of the emission from the carbon layer (degraded by transmission through the crystal and one reflection at the MgO-air interface) and the second term is the contribution due to the radiation from the heated MgO windows.

For heat pulses of short duration, as are experienced in the present experiments, the only contribution which is observed is due to the opaque layer. Almost all of the window remains at room temperature and makes no contribution. Thus, the short pulse becomes in terms of the measured quantities,

$$V_G = \frac{\epsilon X}{1-\tau}\left(V_B - V_C\right) = \left(\frac{\epsilon}{1-\tau}\right)V_2 \approx \left(\frac{1}{1-\tau}\right)V_2 \qquad (17)$$

since the emissivity of the carbon-MgO interface is very close to one. The curve-marked calibration curve in Fig. 10 is calculated from the above equation.

The calibration of the system was checked periodically by measuring the output of the cell when exposed to the black body source, i.e., V_1. This value remained constant throughout the experiment within $\pm$ 4 percent.

From this calibration data an empirical relationship between the calibration signal, V_G, and the black body temperature has been determined in the temperature range of $40°$ to $190°C$. The data fits the following equation,

$$E\,(volts) = C\,T^n \qquad (18)$$

with the constants $C \doteq 5 \times 10^{-5}$ and $n = 2.1 \pm 0.1$.

This calibration procedure has been checked against a dynamic calibration technique by Camac by a measurement of the end wall heat transfer in argon.[8,19] The correspondence of the semi-static (chopper wheel) and dynamic calibration has been assumed in these experiments.

In addition to the calibration of the infrared cell output discussed

above, the time response of the measuring system was determined. Two methods were used. First, a pulse generator was used to impose an electronic pulse through the infrared cell and amplifier onto the oscilloscope. A schematic diagram of this calibration set-up is shown in Fig. 11. In this procedure care must be exercised to be sure that the cell is not loaded down by the pulse generator. The capacitance of the connection of the infrared cell to the amplifier is the critical parameter in determining the rise time of the system. By building the amplifier cathode follower and amplifier almost as a single integrated unit with minimum length bare wire connections, it was possible to reduce the rise time of the system (to 90 percent of the full deflection value) to slightly less than one microsecond.

A second response calibration was performed by the use of periodic light pulse generated by a rotating mirror system. The rise-time of this light pulse itself was approximately one microsecond. The resulting combination of the cell, amplifier and light source gave a rise time of about $1.5\,\mu$sec, which is equivalent to the geometric combination of the two one-microsecond rise times.

The response time of the system can also be tested by a heat transfer test behind a reflected shock in the shock tube. A so-called knife edge model was built for this purpose. This model essentially slices a piece out of the test gas and allows the reflected shock to propagate back in the tube of the model until it reaches the knife edge. The tube was made long enough so that the whole test time is usable in this experiment. Substituting the heat transfer for this geometry, Eq. (7), into the equation for the interface temperature for this situation, i.e., Eq. (4), gives the familiar temperature step function response. Figure 12 shows the oscillograph from such an experiment. The rise time of this record shows the fast response ($1-2\,\mu$sec) required of the gages and the approximately level output thereafter, indicative of the growth of the thermal boundary layer.

For stagnation point heat transfer experiments, the heat transfer starts out as in the above situation and then levels out at a constant value after the viscous boundary layer has been established. The

oscillograms shown in Fig. 13 show this early heat transfer time history clearly. As the example shown from the numerical calculation in the earlier section, the temperature starts to rise when the flow geometry becomes established at times of the order of $8 - 10 \mu$sec. For the constant heat transfer input with time, Eq. (8), the temperature response of the carbon-MgO interface is

$$T(t, x=0) \sim \dot{q}(t) \sqrt{t} \tag{19}$$

as can be seen from Eq. (3). If Eq. (18) is used as the calibration curve, then

$$E(t) \sim \left[\dot{q} \, C T^{n} \right]^{\frac{1}{2}} \sim \dot{q}^{.5} t^{1.05} \tag{20}$$

or the output should be nearly linear with time with the slope being proportional to the square root of the heat transfer rate. This characteristic is shown clearly by the oscillograms shown in Fig. 13.

The oscillograms shown have been reduced to heat transfer time histories by use of the calibration curve, Eq. (18) and the inversion formula, Eq. (10). The heat transfer time history is seen to indicate the characteristic discussed in the previous sections but settles down to a constant value well before the end of the test time, determined by monitoring the visible wavelength radiation with a photomultiplier.

As the infrared heat transfer gage measures the temperature of the carbon layer on the surface of the MgO window during its exposure to the total invironment, it responds to both convective and radiative heating. In order to differentiate between these two heating mechanisms, the reflective properties of the gage surface must be known. For metallic film evaporated the reflectance is generally quite high and, consequently, radiative heating is rejected quite efficiently since the gage is heated by q (convective) $+ \epsilon$ q (radiative). Figure 14 shows the reflectance of freshly evaporated films of the various materials used in the present experiments as compiled in Refs. 20 and 21.

In the process of making the infrared gages, the metallic films

were deposited on the chemically decomposed carbon layers which, in turn, were on a slightly roughened MgO crystal. The optical characteristics achieved by this process could well be considerably different from the literature values of evaporated films. In addition, it was also questioned whether the metallic surfaces deteriorated with time when exposed to ambient conditions. Generally gages were of the order of one day old when used in the shock tube and the handling specifications during this interim were questioned.

The total reflectance of the various coatings was measured by a Beckman Dk-2 (Extended range) Spectrophotometer,[22] useful over the wavelength range of 0.2 to 2.6 microns. In order to deduce absolute values out of the measurements, corrections were required because the inside of the integrating sphere of the instrument was coated with MgO to provide a pure white reflecting surface.[23] The results of these measurements are presented in Fig. 15. It is clear that the plating procedure used degrades the reflectance somewhat but does not change the basic pattern of very high reflectance for metallic films and low reflectance for the carbon.

For the present series of experiments the effect of radiative heat transfer was small. For the stagnation point experiments radiation merely manifests itself as an added increment of constant heat transfer, q_{rad}. As such it is very difficult to differentiate from the convective heating. Estimates of the magnitude of this effect are shown in Fig. 16, using Ref. 24 for the intensity of the radiative flux, for the range of conditions of the present experiment. It can be seen that with an average surface emissivity of approximately $.12 \pm .05$ it should be possible to keep radiative effects down to a maximum level of 2 percent This is probably well within the scatter of the present experiments and the estimate is high because it is known that Ref. 24 overestimates the radiation in this regime by about a factor of two or three.[25]

For the reflected shock geometry afforded by the knife edge model, the radiative contribution is easier to isolate from the convective effects. Due to the growth of the thermal boundary layer, the convective heat transfer rate falls inversely with the square root of

time.   The radiative heating will grow directly with time due to the increasing thickness of the radiating gas region as long as the hot gas does not become opaque.   A linear growth of the heating rate will result in a surface temperature increasing as the 3/2 power of time and an infrared gage output rising approximately with time cubed.   Such a signal is readily distinguishable from the normal constant output shown in Fig. 12.

The knife edge model thus becomes a more useful tool for total radiative heating measurements from gases under these conditions. A typical oscillogram from an experiment in which significant radiation was present is shown in Fig. 17.   The gage used here was overcoated with carbon, i.e., it was triple coated, carbon-metal-carbon, to maximize the emissivity of the surface. The temperature response of the knife edge model to the radiative heating predicted from Ref. 24 is shown in Fig. 18.   It is seen that the effects are clearly measurable, even with realistic values of emissivity and the new data on air radiation.

SECTION V

HEAT TRANSFER RESULTS

The heat transfer data from the present series of experiments are shown in the Fig. 19. The initial shock tube pressure was 0.25 mm Hg, the gas was room air, and the incident shock wave velocities ranged from U_s = 7 to U = 10.0 mm/μsec, simulating[1] flight at altitudes of approximately 140,000 ft and a simulated velocity of up to approximately 50,000 fps. Only data points from experiments during which at least 8 μsec of test time were measured by one of the methods stated in the Ref. 1 have been used in view of the response requirements discussed in the previous sections.

Stagnation point convective (aerodynamic) heat transfer data were measured mostly on sphere-cone models with nose radii R_N = 1.27 cm and R_N = 1.905 cm. Majority of the test runs were made with aluminum and gold reflective films overcoating the carbon gage. A few data points were obtained using Nichrome alloy as the evaporated surface film. The infrared gage coatings lasted only for one shock tube run and usualy deteriorated after approximately 30 μsec, possibly due to impact of impurities and residues of the driver gas causing the film to become transparent. This was very plainly evident by the almost instantaneous rise of the signal beyond the range of the amplifier and scopes. The data have been compared with results calculated from the Fay and Kemp binary diffusion model for ionized diatomic gases.[4] Figure 19 also shows the curve fit of the data (which had a root-mean-square deviation of 0.13) obtained from measurements with calorimeter gages reported in Ref. 1. In general, the average values of the present data appear to follow the theoretical predictions of equilibrium air somewhat more closely and majority of the data points thus lie slightly above the results of the Ref. 1.

There appears to be no significant difference between the data obtained with aluminum and gold films covering the carbon gage. This is in agreement with Collins and Spiegel[3] but in contrast to the result of gage material reported by Gruszczynski and Warren.[7] The nickel alloy, Nichrome, results also fell directly in the group of the data from the other materials. In view of the fact that these experiments were all performed at the lowest initial pressures used in any of these experiments, surface reactions should certainly have been present. The obvious advantage of this experiment over the above references is that a single gage calibration is used for all the surface materials and, consequently, differences in the measurements, if present, could be directly attributed to surface-gas interactions. Consequently, it must be assumed that the gage surface material does not have an influence on the convective heat transfer.

The heat transfer measurements reported here must be viewed with the same reservations with respect to the state of the test gas as discussed thoroughly in Ref. 1. Briefly, the test gas is assumed to be in equilibrium. Experimental measurements of the visible radiation show this to be a good assumption for dissociation of the inviscid flow at the stagnation point. Our present knowledge of recombination rates indicates that the boundary layer may involve some freezing but not to a degree sufficient to influence the heat transfer rate.[1] With respect to ionization, estimates of the degree of completion of these processes were also made in Ref. 1. Recent experiment of Wilson[26] have tended to confirm these estimates. Wilson finds that behind strong shock waves the ionization mechanism is analogous to the process suggested by Petschek and Byron.[27] In the air case, the initial ionization is provided by the atom-atom reactions, as per Lin,[28] and the impact process takes over as soon as sufficient electrons are produced. The result is that the time to achieve equilibration, in terms of the number of ambient mean-free-times, does not change radically up to shock velocities as high as 12 mm/μsec, thus confirming the extrapolations used in Ref. 1 and adding confidence to the assumption that ionization processes are also in equilibrium in these experiments.

SECTION VI

SUMMARY AND CONCLUSIONS

Heat transfer measurements made with an infrared heat transfer gage have been presented. The value of these measurements is, (1) a new technique has been developed for producing such measurements which is significantly different from the commonly used calorimeter resistance thermometer, (2) the measurements obtained with the new technique essentially duplicate and consequently verify the results of several authors achieved with calorimeter gages, and (3) variations of the surface material of the surface undergoing heat transfer did not alter the resultant heat transfer rates, showing conclusively that surface effects are not important under the experimental conditions.

ACKNOWLEDGMENT

$U_S = 8.0 \text{ mm}/\mu \text{ sec}$

$R_N = 1.905 \text{ cm}$

$P_I = 0.025 \text{ cm Hg}-\text{AIR}$

$\dot{q}_e \sqrt{t} = 19.1 \text{ (WATT}/\text{CM}^2) \sqrt{\text{SEC}}$

$\dot{q}_S = 10 \text{ KW}/\text{CM}^2$

(FAY & KEMP EQ. AIR-15%)

$\dot{q} - \text{kW}/\text{cm}^2$

TIME $-$ SEC X 10^{-6}
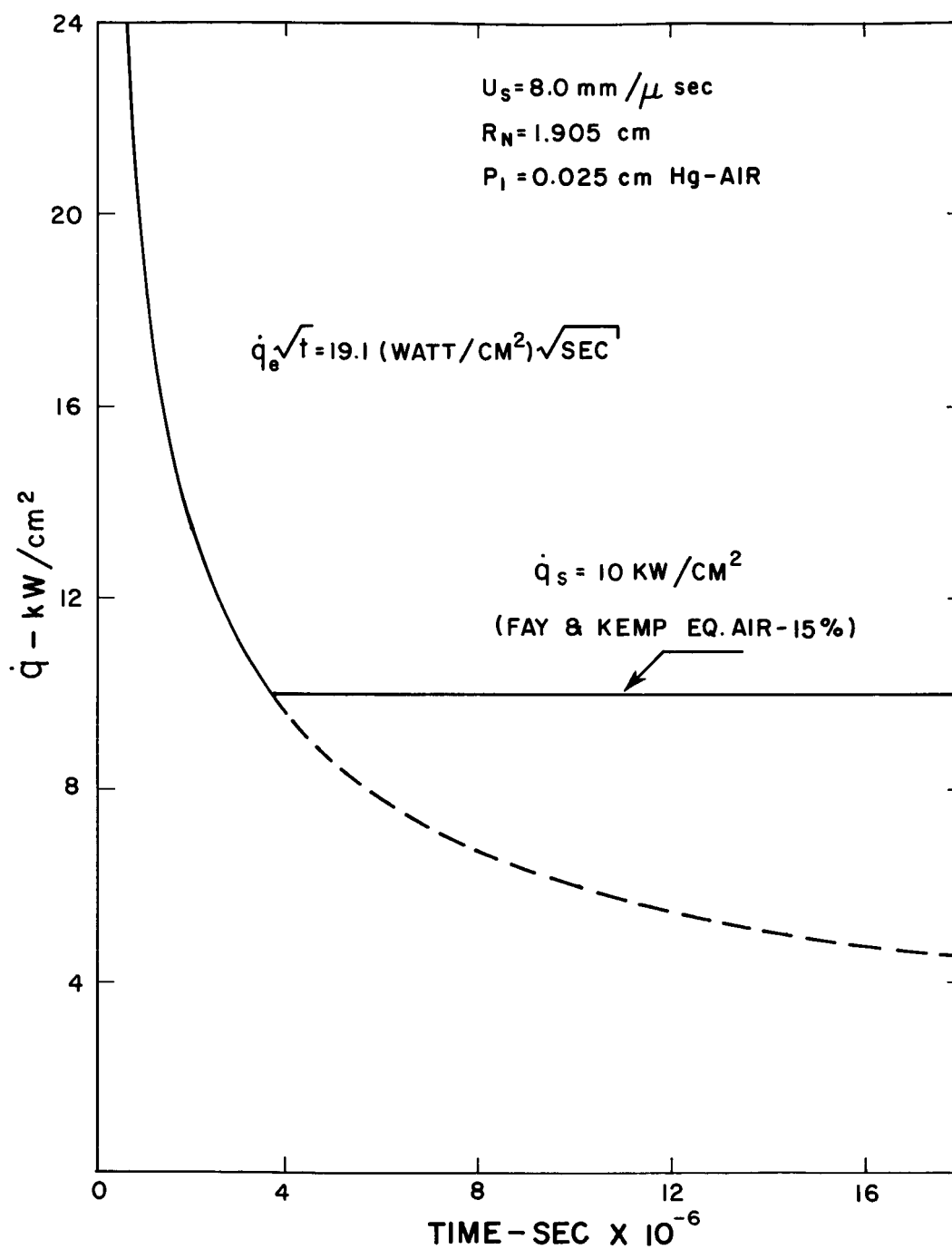
Fig. 1   Estimate of transient heat transfer time history at the stagnation point of a spherical nosed body.

-24-

A2577
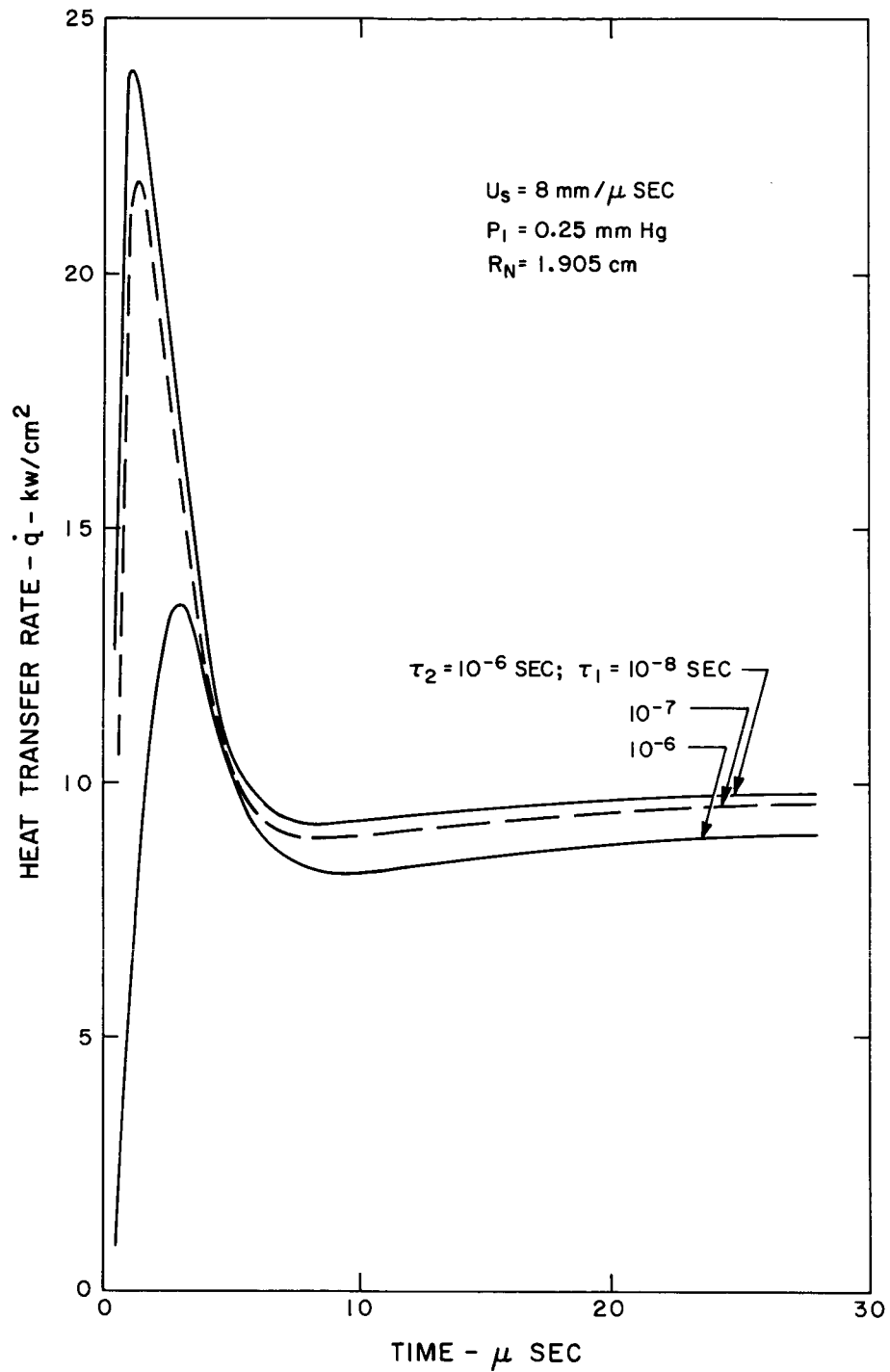
Fig. 2   Effect of thermal response of the window-carbon interface, τ_1 on stagnation point heat transfer time histories.
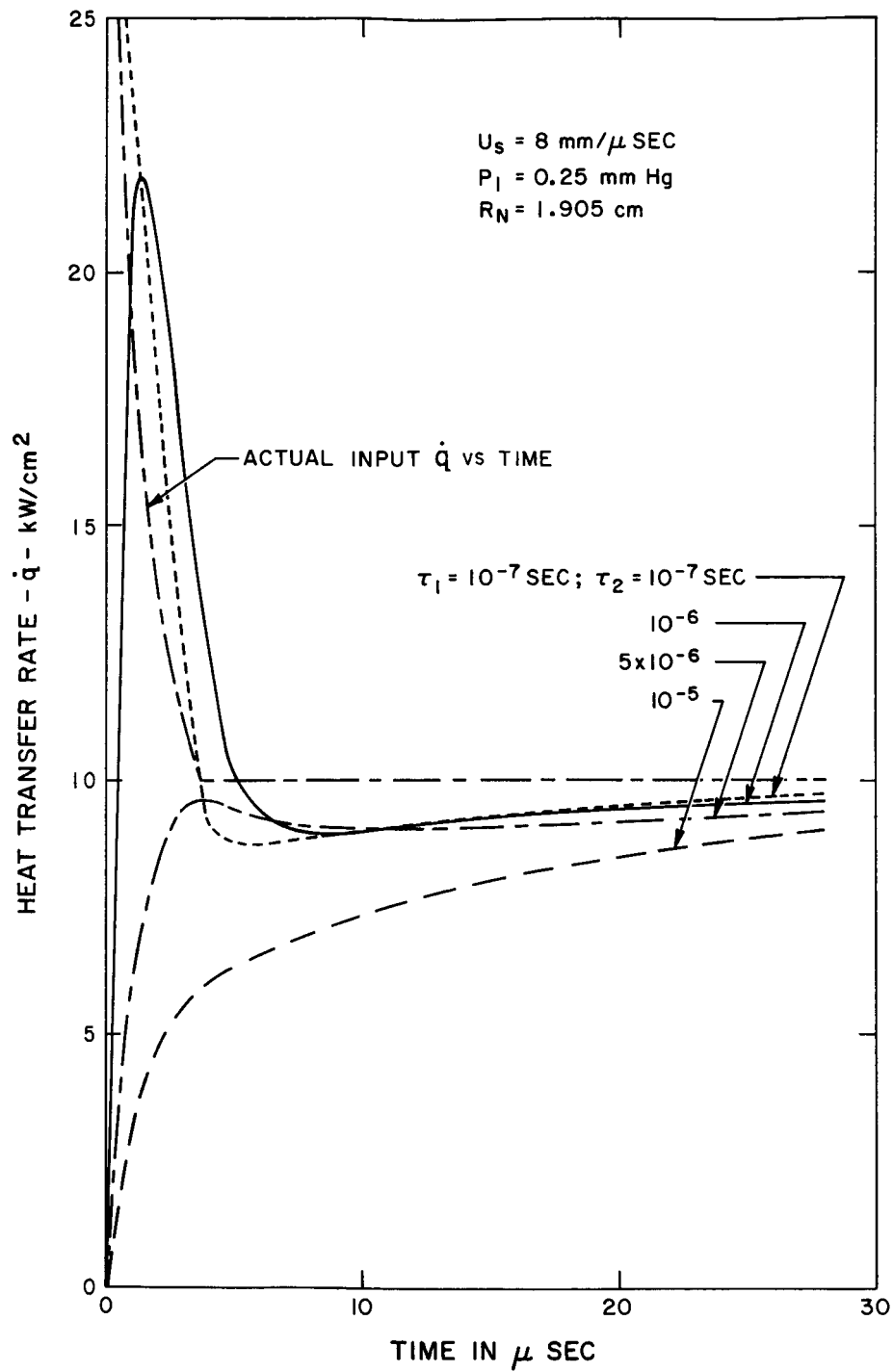
Fig. 3   Effect of infrared gage circuit response time, τ_2, on stagnation point heat transfer rate time history.
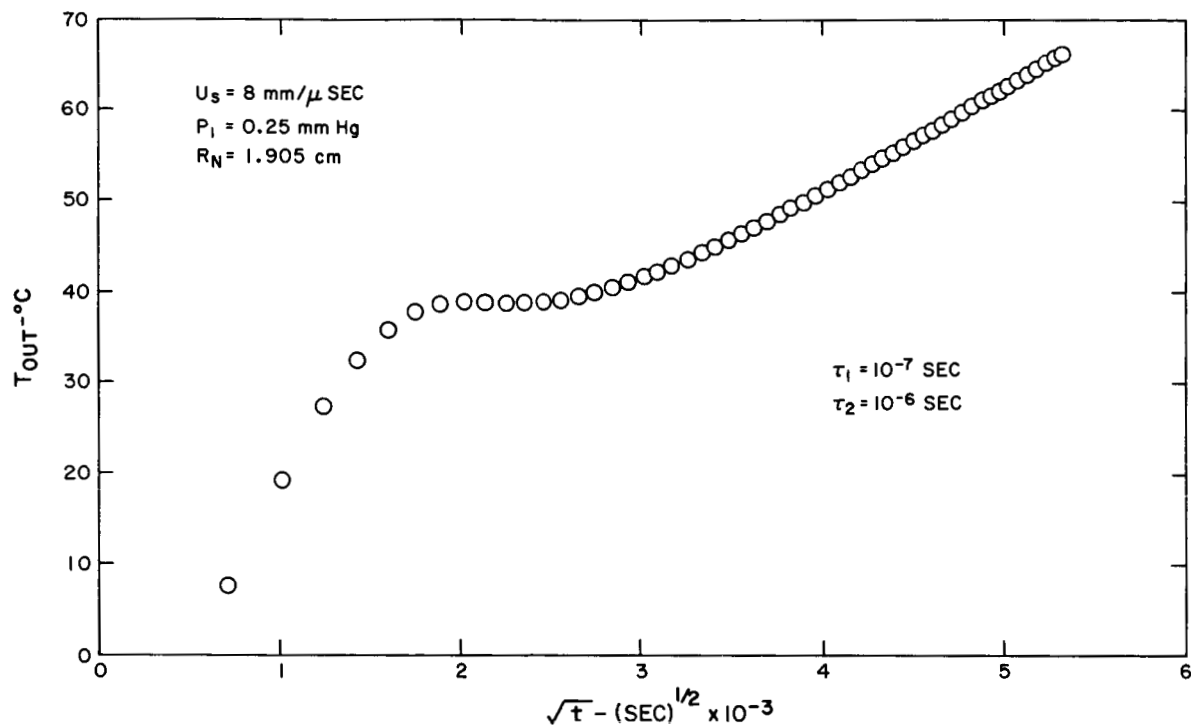
Fig. 4   Degraded temperature time history calculated for the infrared detector output signal due to the heat transfer input shown in Fig. 1 for response times τ_1 and τ_2 typical for this experiment.
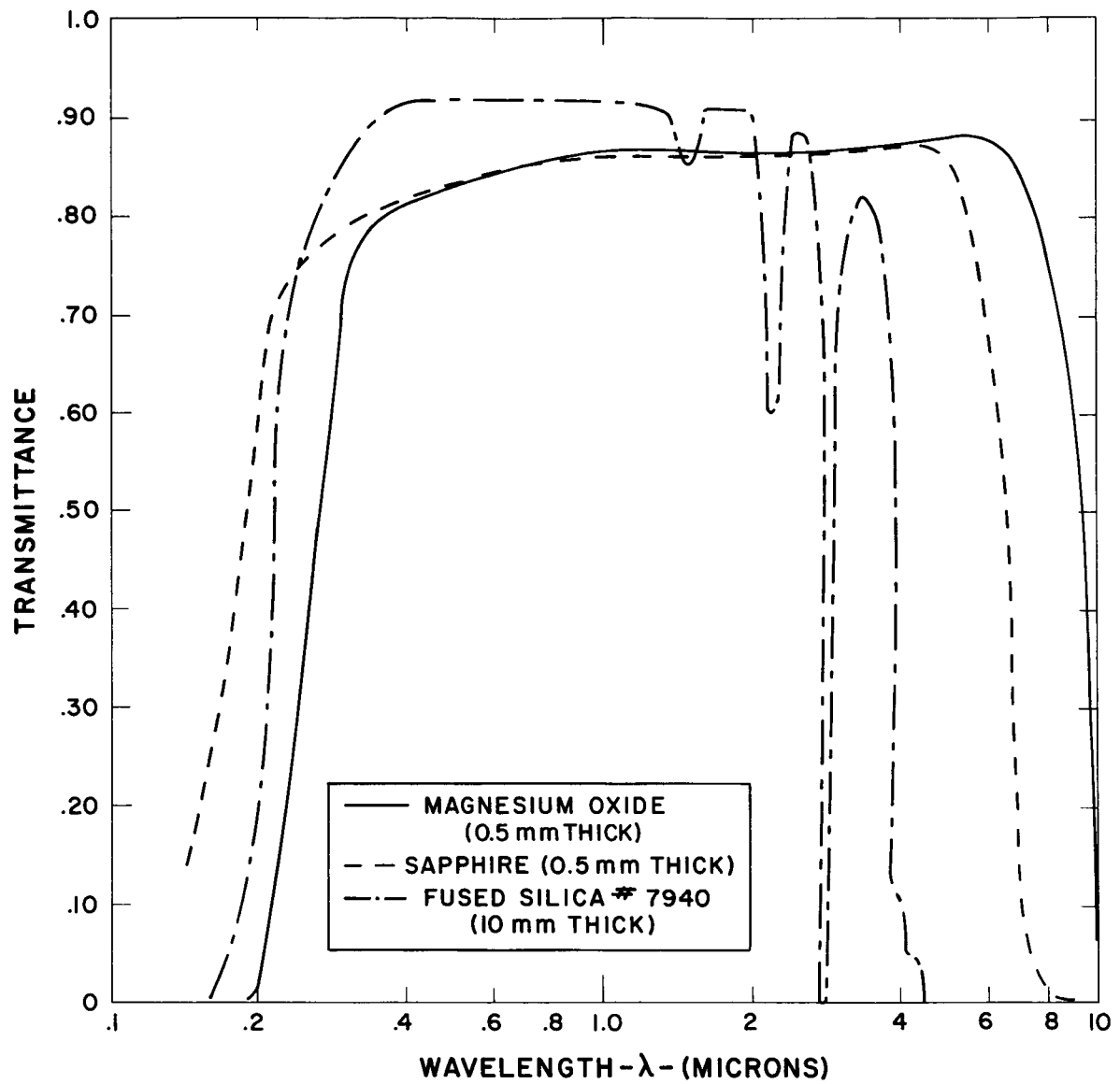
Fig. 5   Transmission of fused magnesium oxide (MgO) windows (0.5 mm thick).

A1765
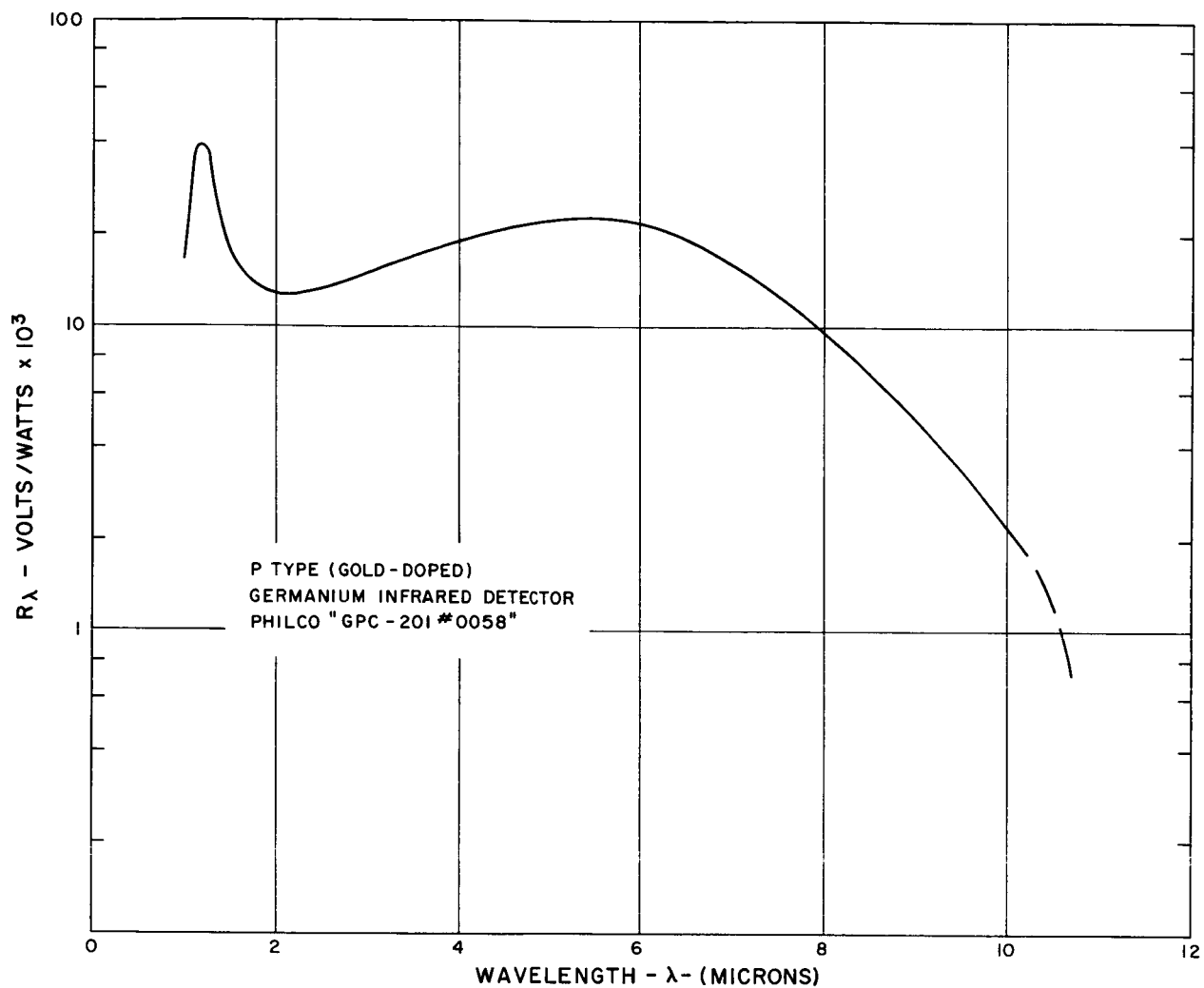
Fig. 6   Spectral responsibity of the Philco GPL-201 gold-doped germanium infrared detector used.

A2582

GOLD DOPED
GERMANIUM
INFRARED
DETECTOR CELL

RING
MIRROR

SOLID
MIRROR

30°

.500R
.750R
1.000R
1.500R

.085
DIA.

.020

MgO WINDOW
DIMENSIONS

REFLECTION
MIRROR
ASSEMBLY

CARBON COATED
FUSED MAGNESIUM
OXIDE (MgO)

R

3.00"
DIA.

CASSEGRAIN OPTICAL
MIRROR ASSEMBLY

ARC-DRIVEN
6" DIA.
SHOCK TUBE

SUPPORT FLANGE
FOR SHOCK TUBE

VISIBLE PM FOR
OPACITY CHECK
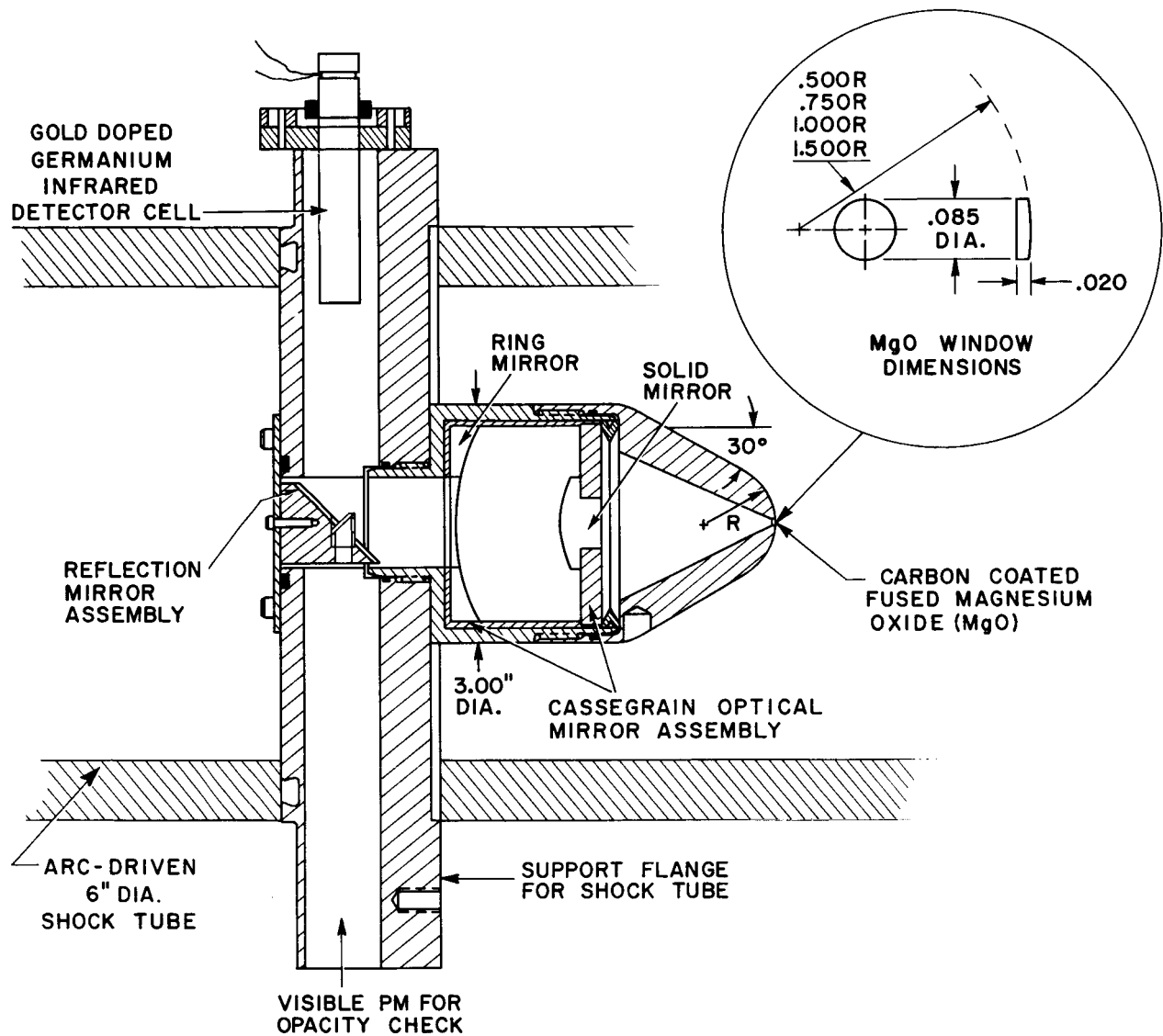
Fig. 7   Drawing of the infrared carbon gage, optical system and
detector built into shock tube model.

A1324
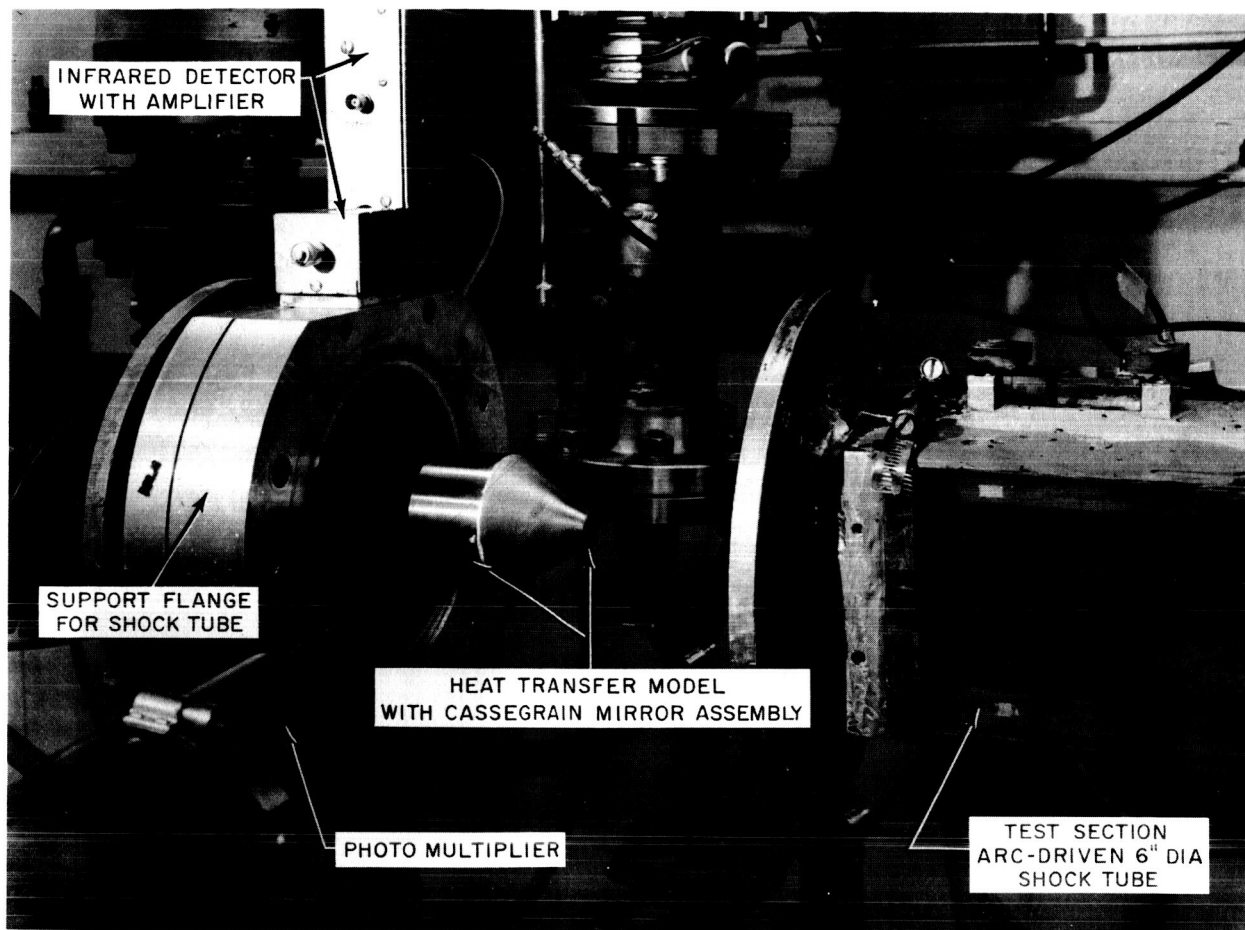
Fig. 8   Photograph of the infrared heat transfer gage, detector and
model mounted in the 6-inch diameter electric arc-driven
shock tube.

A2583
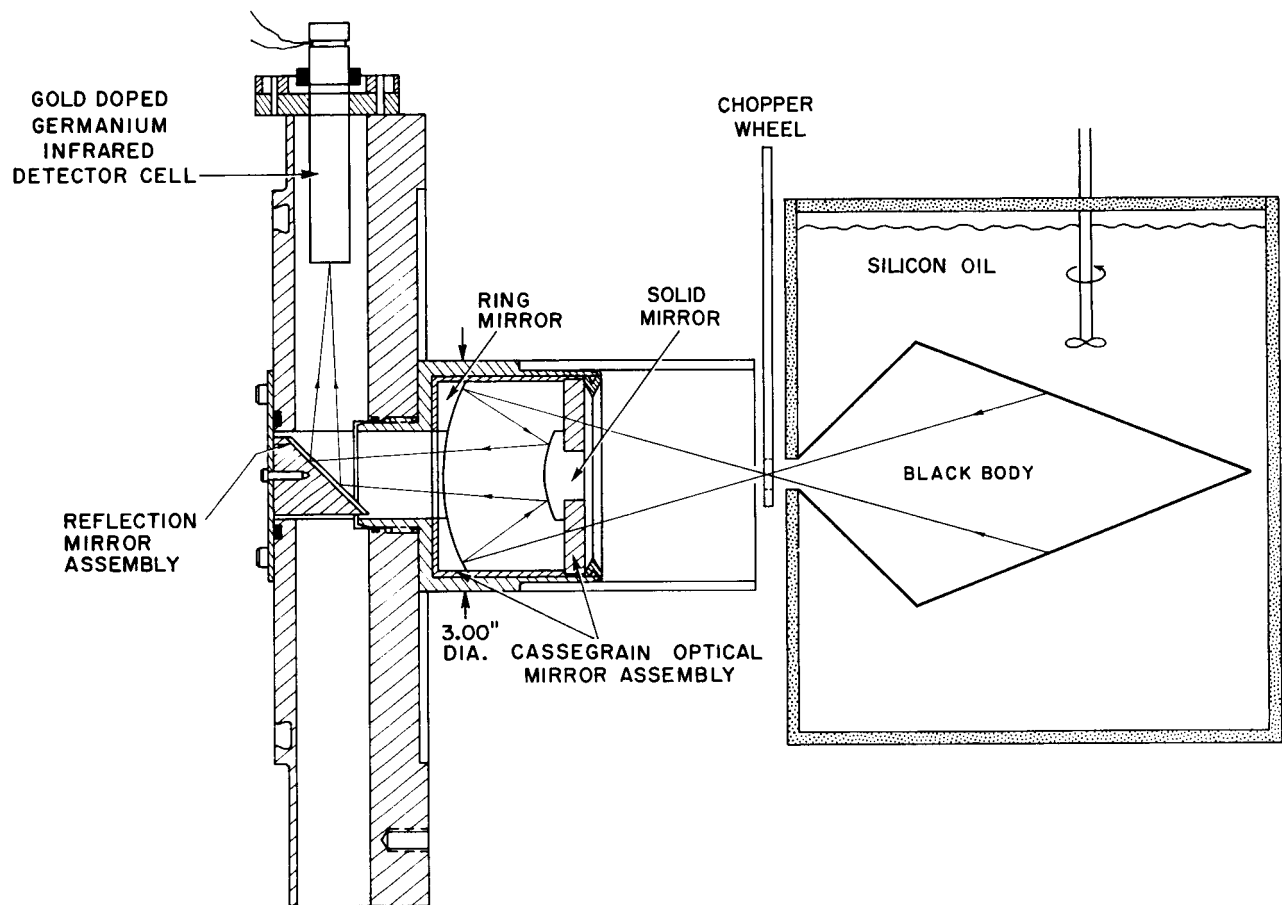
Fig. 9   Calibration setup of infrared heat transfer gage assembly using the black body source. Radiation from the cavity is imaged by the gage optical system on the infrared cell.
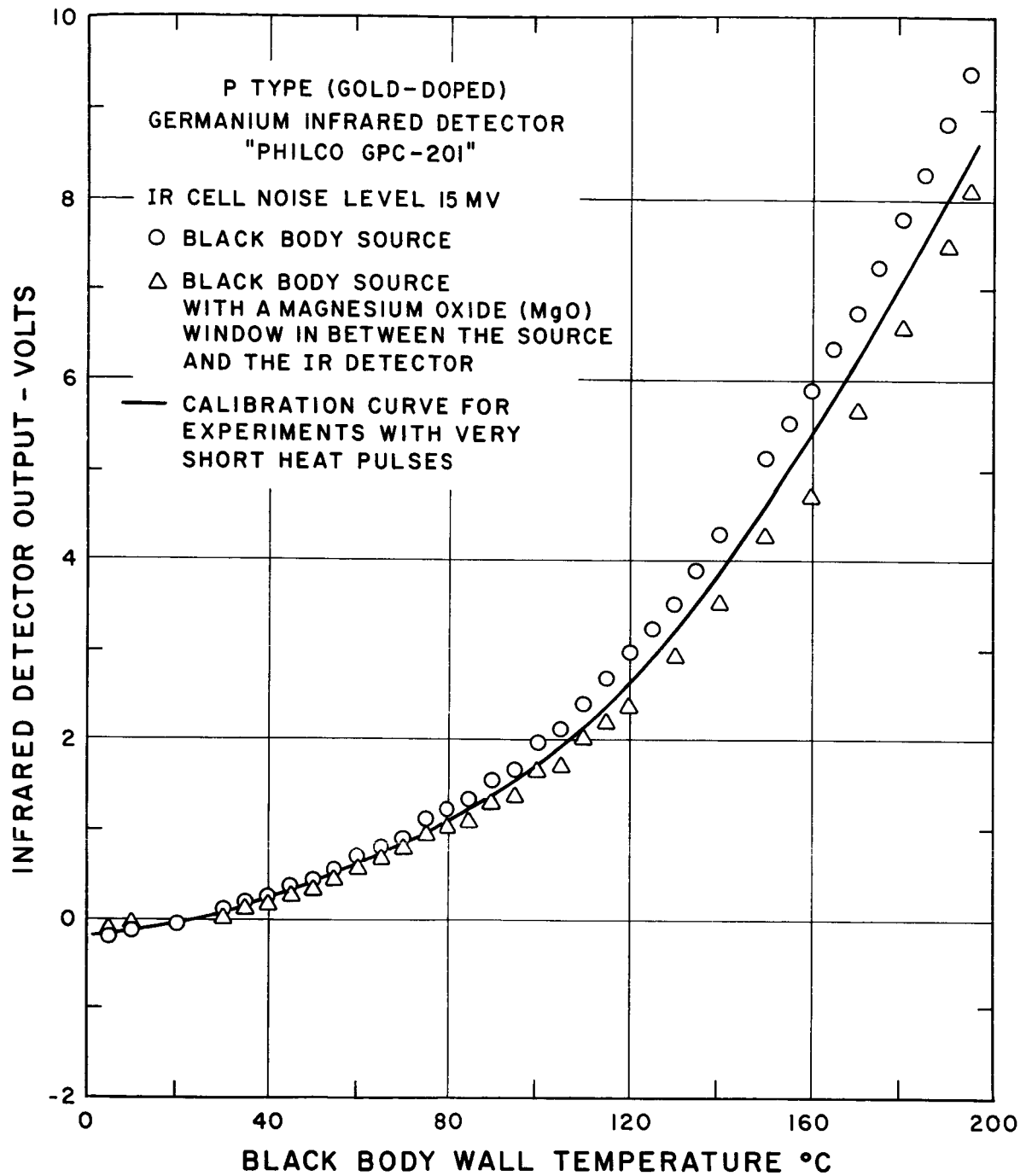
A2584

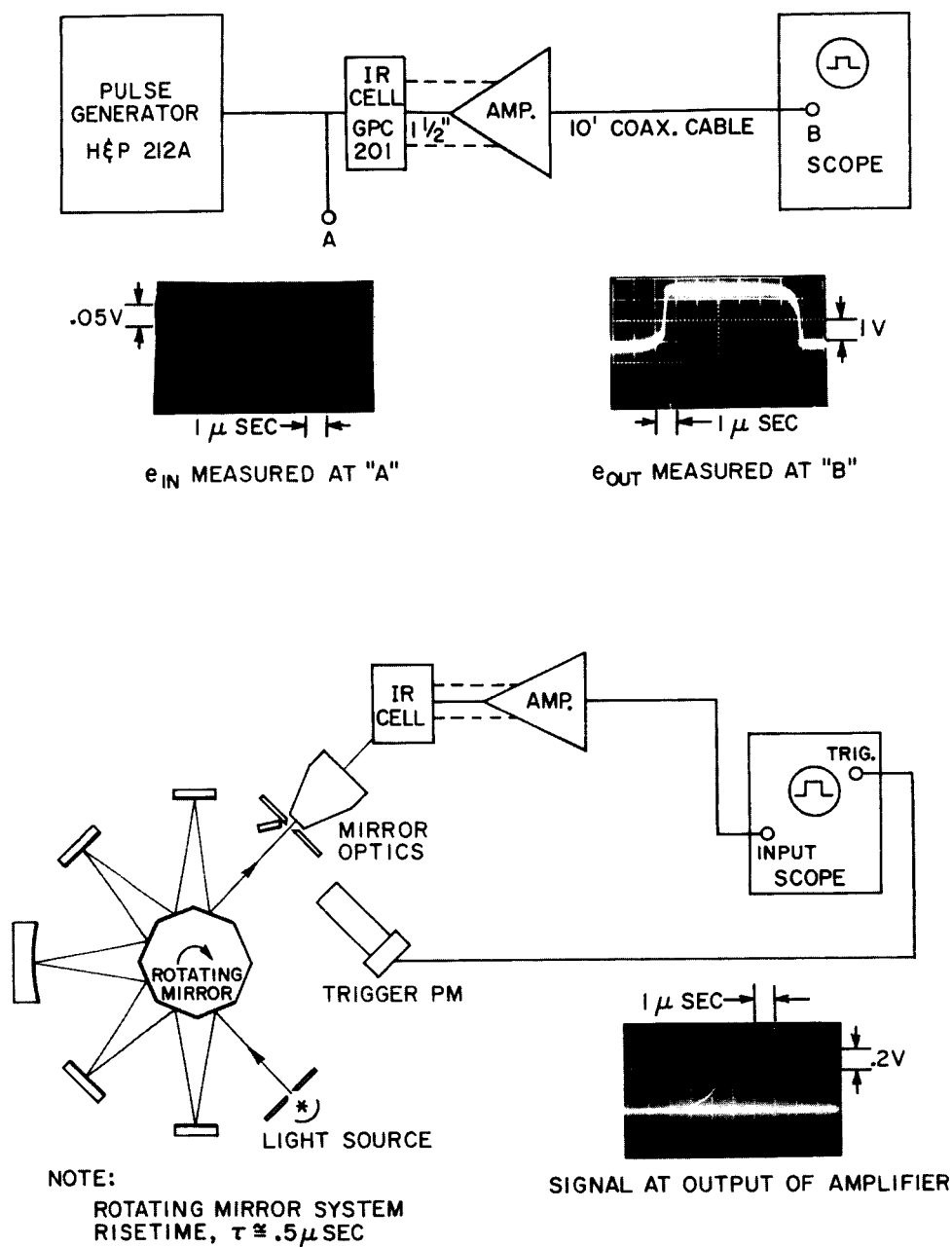Fig. 10   Calibration curves of the infrared heat transfer gage system.

A2485

PULSE
GENERATOR
H&P 212A

IR
CELL
GPC
201 | 1½"

AMP.

10' COAX. CABLE

B
SCOPE

A

.05V

1 μ SEC

e$_{IN}$ MEASURED AT "A"

1 V

1 μ SEC

e$_{OUT}$ MEASURED AT "B"

IR
CELL

AMP.

TRIG.

INPUT
SCOPE

MIRROR
OPTICS

ROTATING
MIRROR

TRIGGER PM

LIGHT SOURCE

1 μ SEC

.2V

SIGNAL AT OUTPUT OF AMPLIFIER

NOTE:
   ROTATING MIRROR SYSTEM
   RISETIME, $\tau \cong .5 \mu$ SEC

Fig. 11   Schematic diagrams of two set-ups used for measuring the
time response characteristics of the infrared heat transfer
gage system, one using an electronic pulse and one a light
pulse generator.

-34-

A2486

INFRARED CELL AND PM OUTPUT IN VOLTS
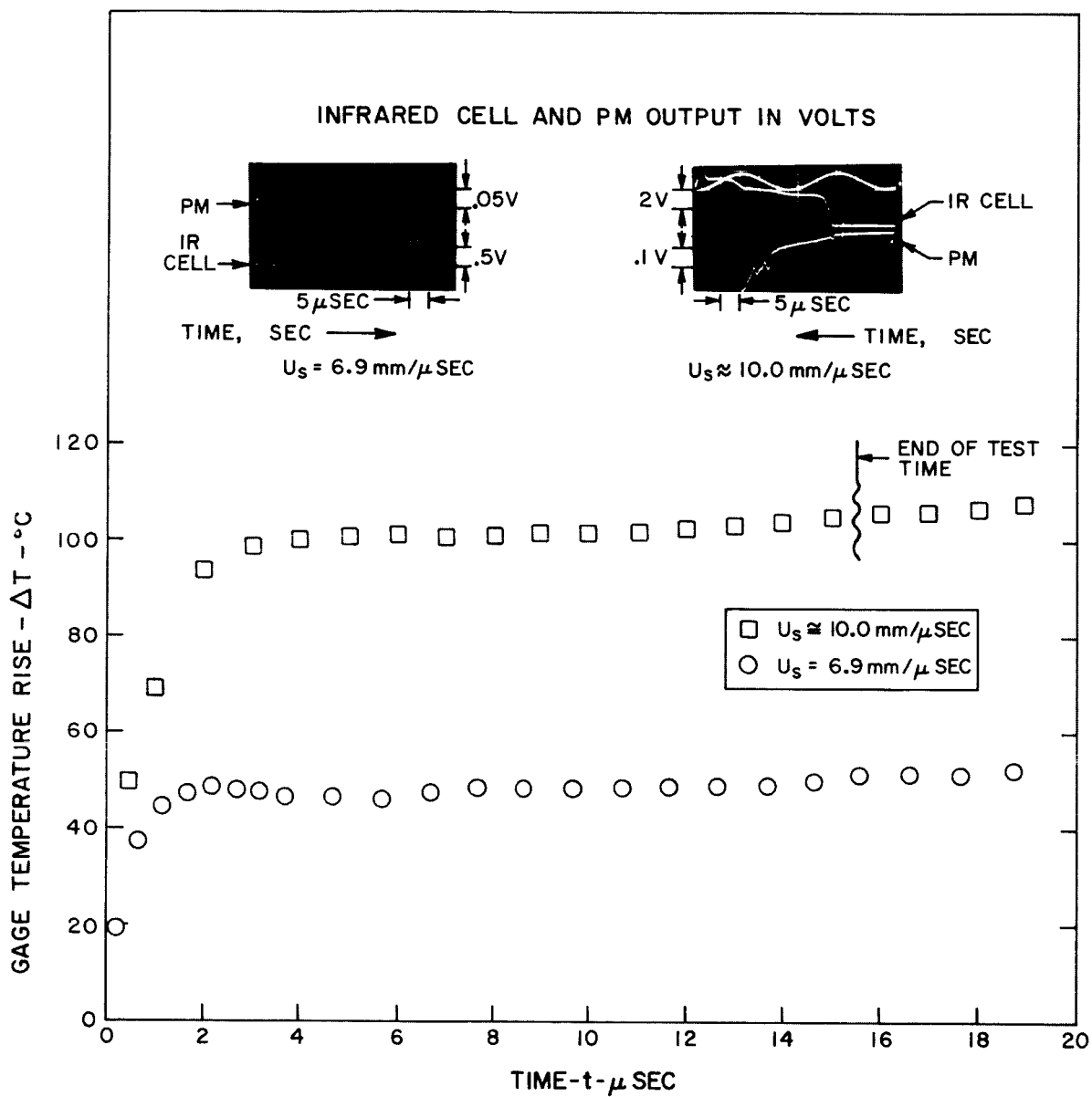
Fig. 12   Oscillograms of the data measured at two shock velocities
with the infrared heat transfer gage in the knife edge model
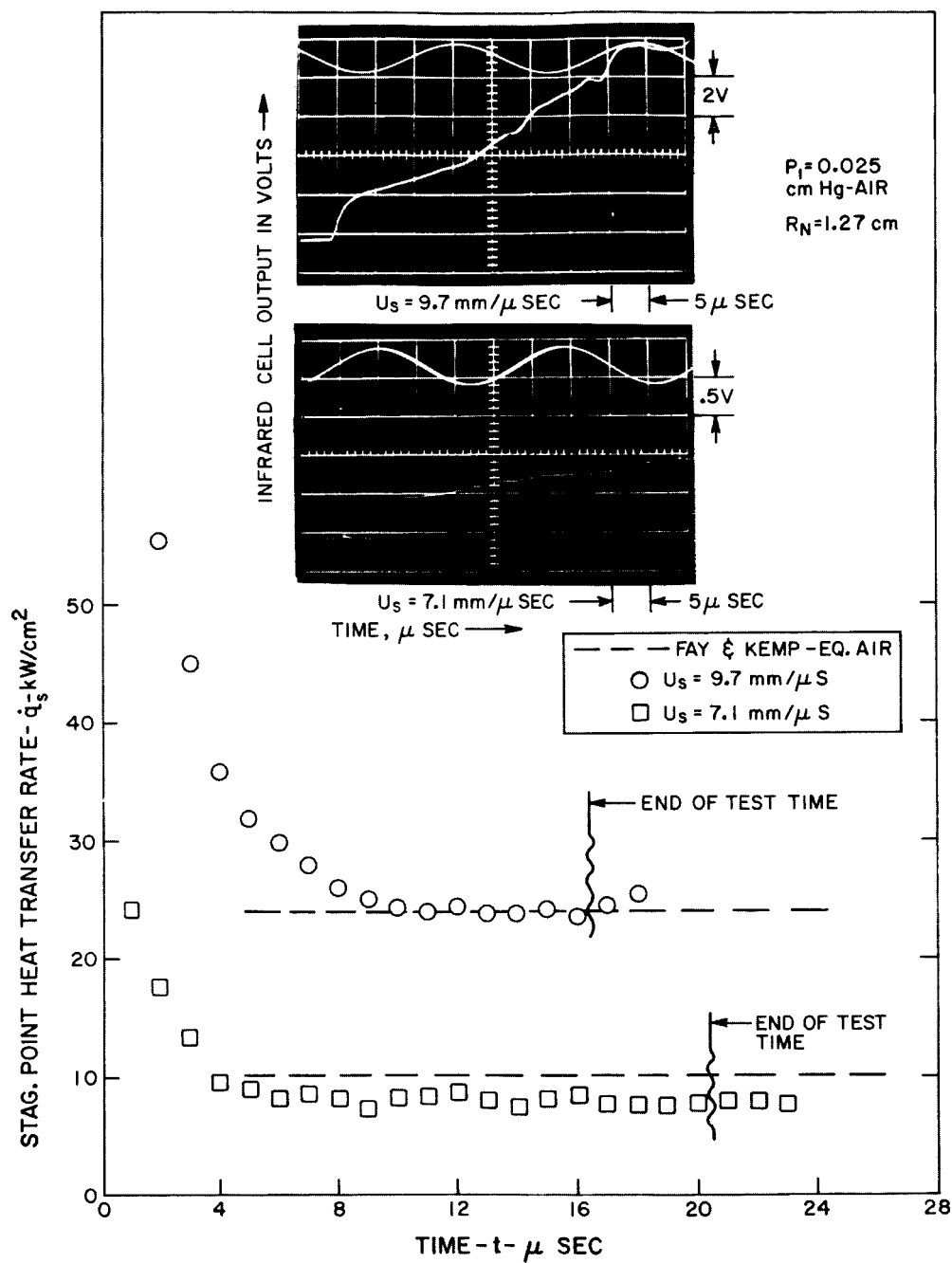duplicating the shock tube end wall.

Fig. 13   Oscillogram of the data obtained at the stagnation point of the spherical nosed model measured with the infrared heat transfer gage at two different shock velocities.
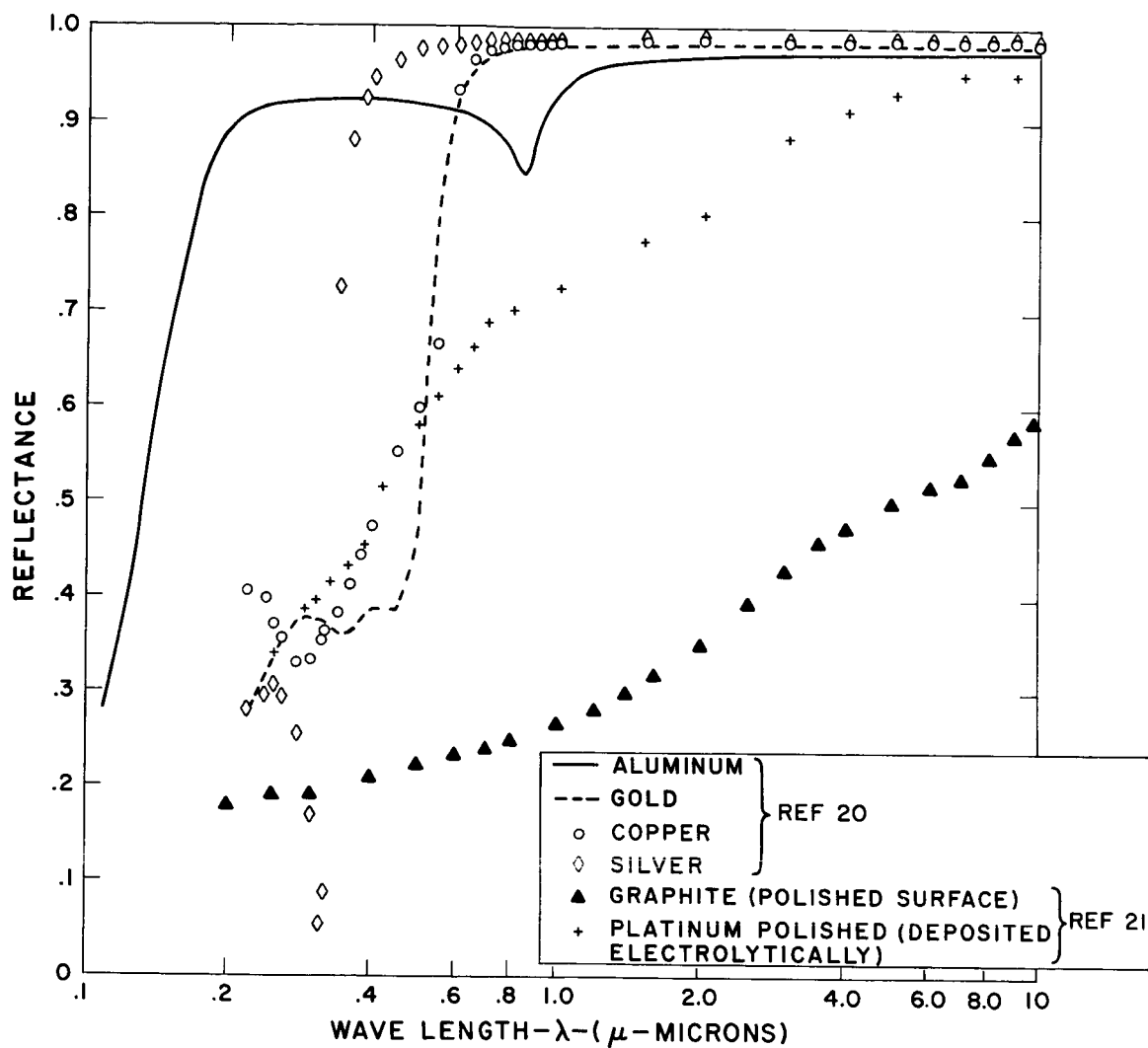
-36-

Fig. 14   Reflectance of freshly evaporated metal films of the various materials used in the experiments from Refs. 20 and 21.
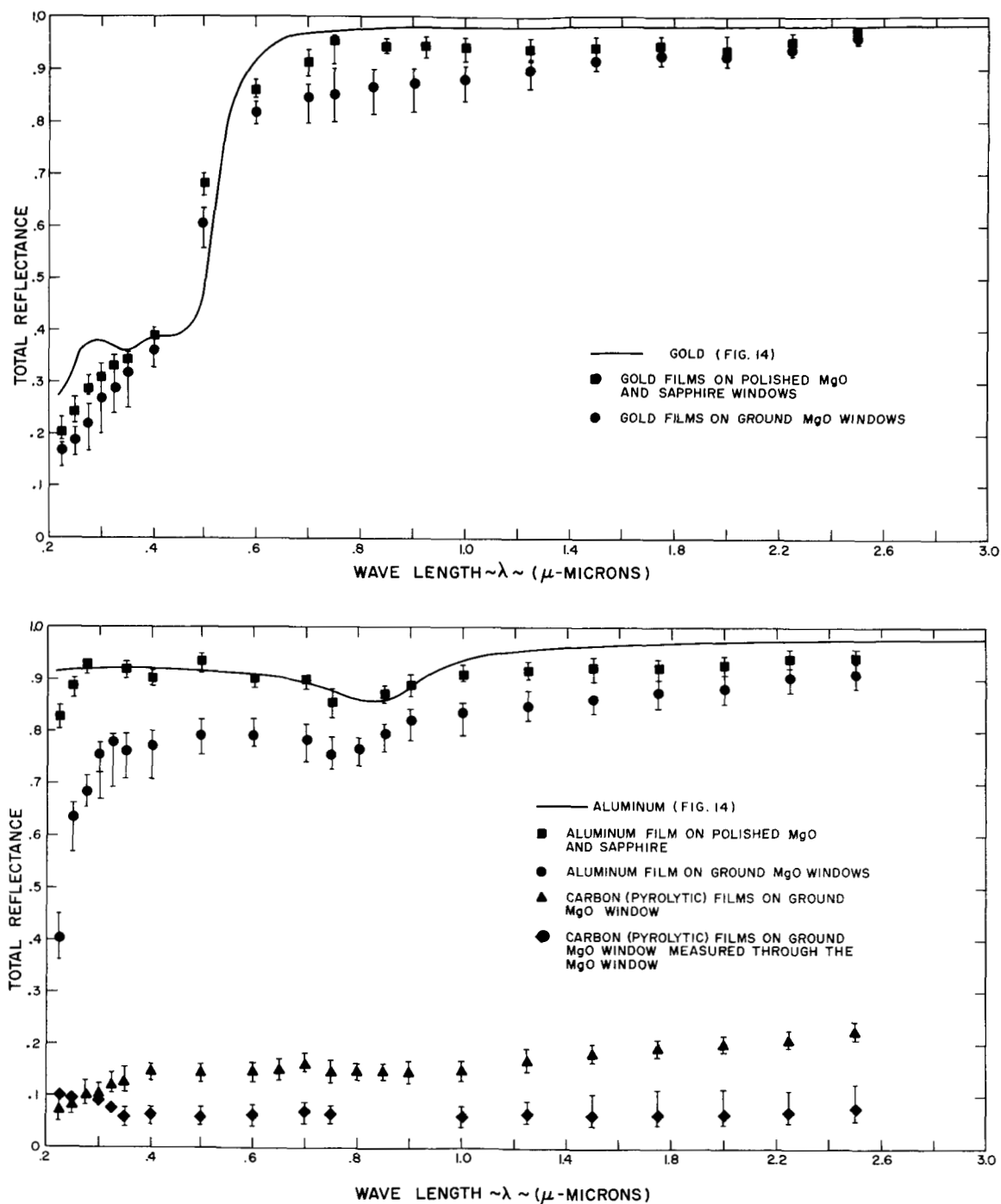
A2589

Fig. 15   Total reflectance measured for evaporated metal coatings
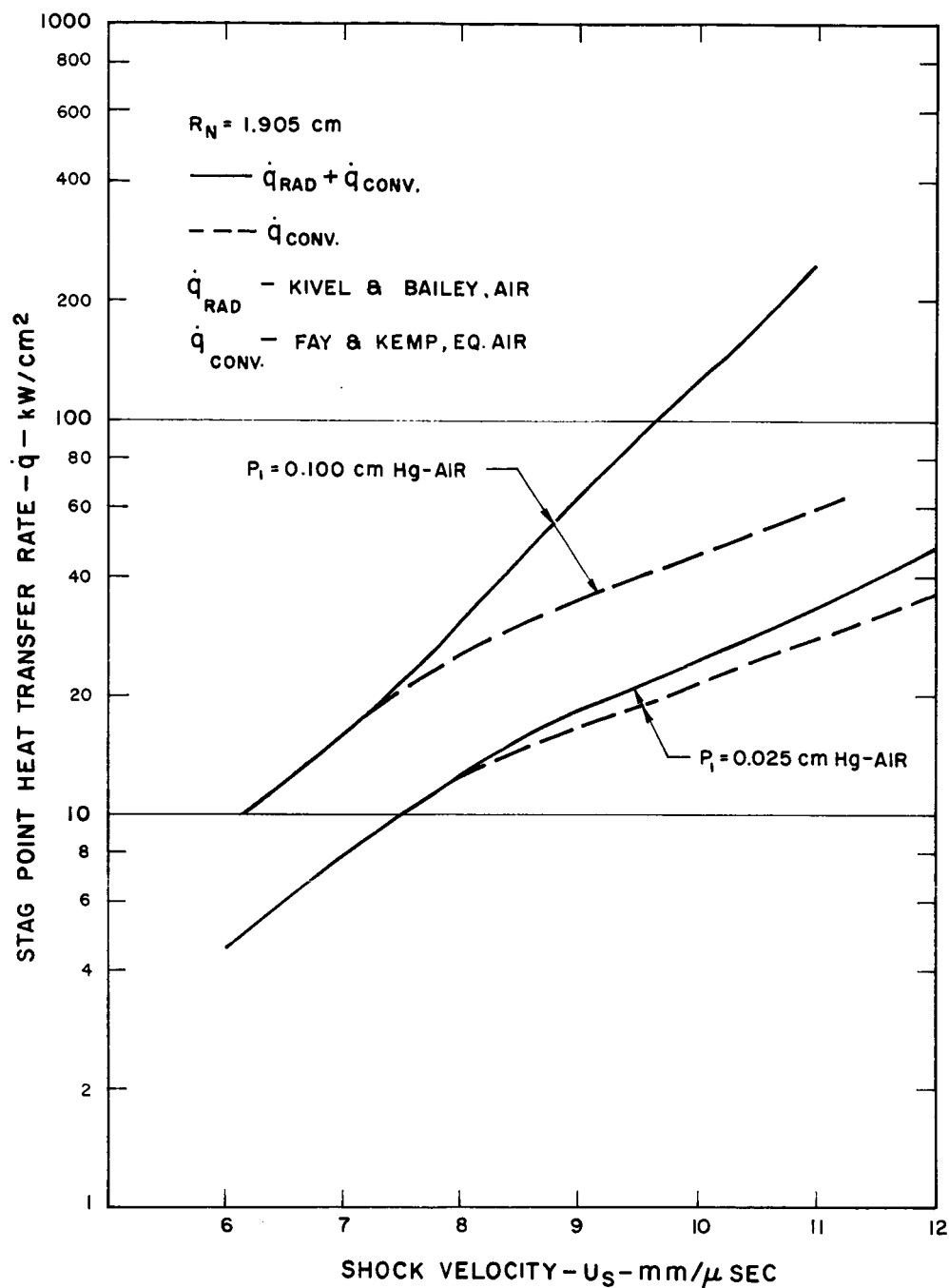deposited on the carbon layer on an MgO window.

Fig. 16   Radiative and convective heating at the stagnation point of a model. Convective heating was calculated from Fay and Kemp;[4] equilibrium boundary layer and radiative heating was computed from Kivel and Bailey[24] assuming 100% absorption by the gage.
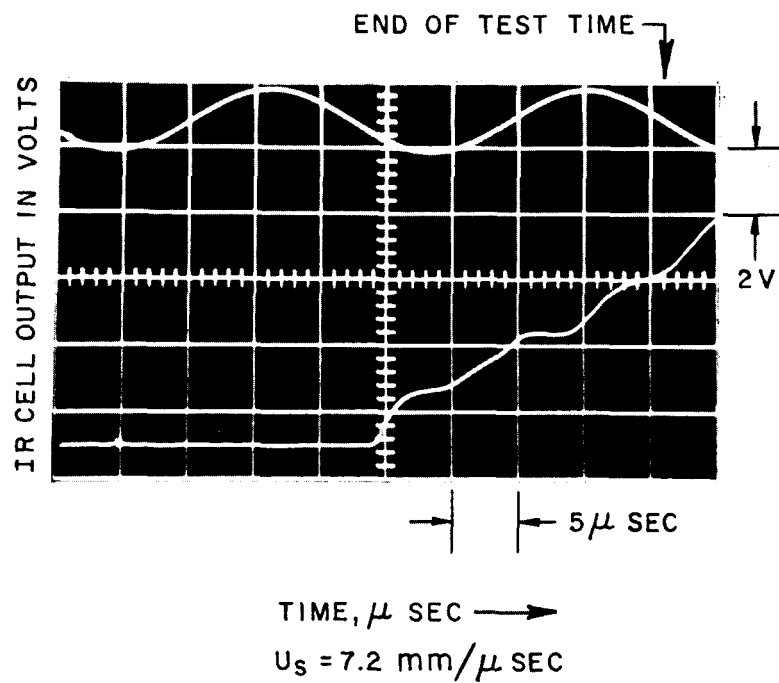
A2591

Fig. 17   Oscillogram of data obtained from carbon-coated infrared gage in the knife edge model.
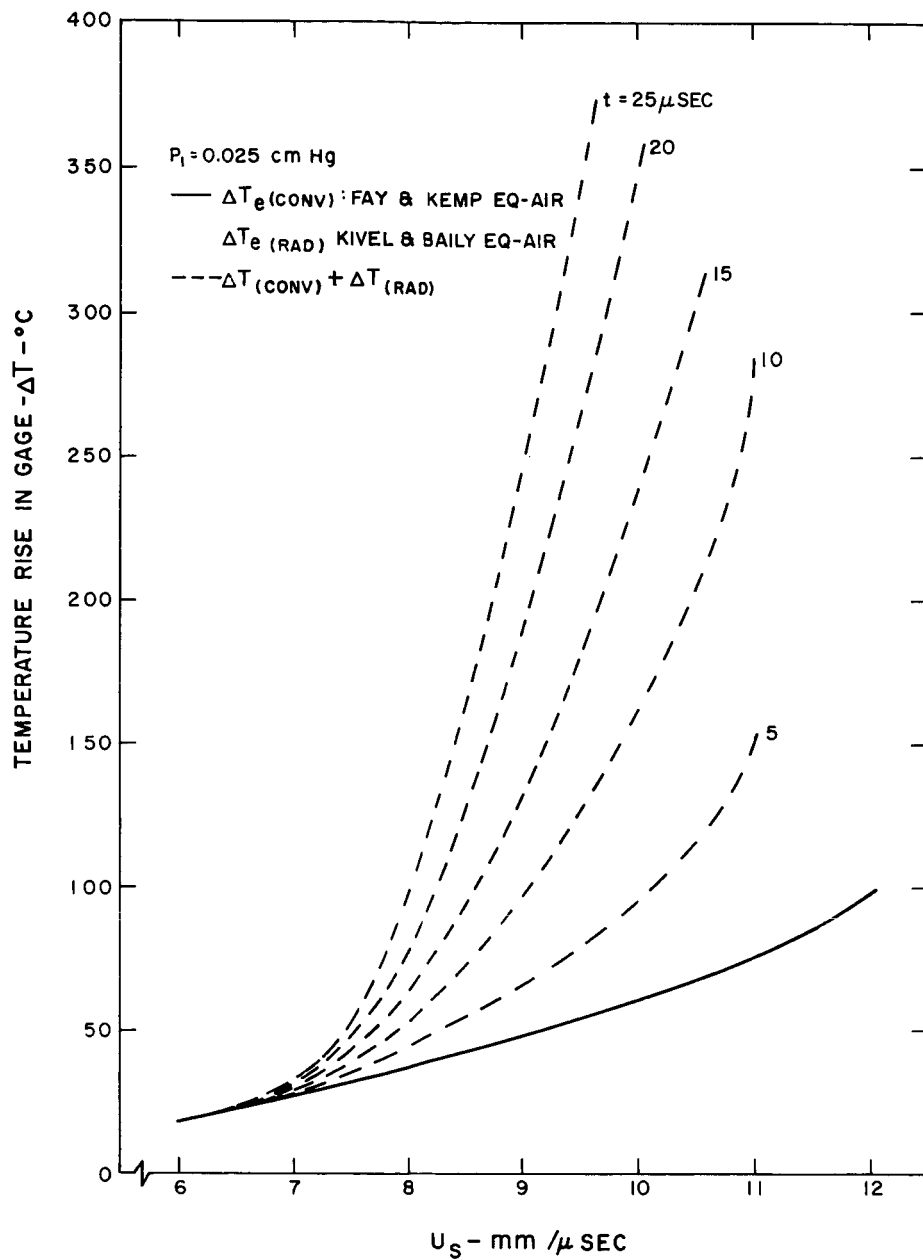
-40-

Fig. 18   Calculated temperature response of the infrared gage in the knife edge model based on radiative heating estimates from Ref. 24.
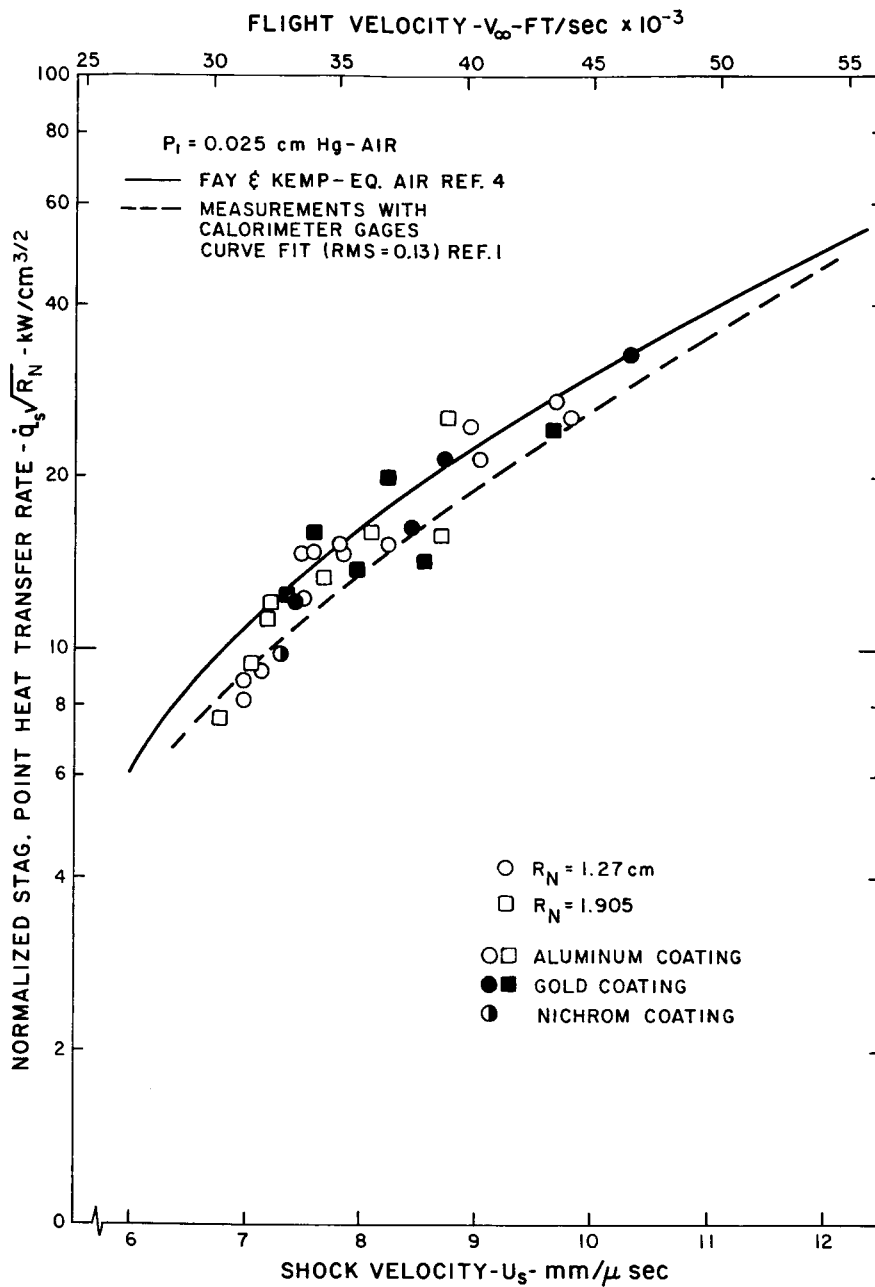
A2593

Fig 19   Summary plot of stagnation point heat transfer rates measured with the infrared heat transfer gage.

REFERENCES

1. Rose, P. H. and Stankevics, J. O., "Stagnation Point Heat Transfer Measurements in Partially Ionized Air," AIAA Jour. 1, 2752-2753 (December 1963), also Avco-Everett Research Laboratory Research Report 143, April 1963.

2. Hoshizaki, H., "Convective Heat Transfer Measurements at Superorbital Speeds," Lockheed Missiles and Space Division, Rept. No. 6-90-62-50, June 1962.

3. Collins, D. J. and Spiegel J. M., "Effects of Gage Material on Convective Heat Transfer," AIAA Jour., 2, 777-778 (April 1964).

4. Fay, J. A. and Kemp, N. H., "Theory of Stagnation Point Heat Transfer in a Partially Ionized Diatomic Gas," AIAA Jour., 2, 2741-2751, also Avco-Everett Research Laboratory Research Report 144, April 1963.

5. Pallone, A. and Van Tassell, W., "The Effects of Ionization on Stagnation-point Heat Transfer in Air and in Nitrogen," Avco Research and Advanced Development Division, RAD TM 62-75 (September 1962)

6. Hoshizaki, H., "Heat Transfer in Planetary Atmospheres at Supersatellite Speeds," ARS Jour., 32, 1544-1552 (1962).

7. Gruszczynski, J. S. and Warren, W. R., "Experimental Heat Transfer Studies of Hypervelocity Flight in Planetary Atmospheres," AIAA Preprint 63-450 (August 1963).

8. Camac, M. and Feinberg, R. M., "High Speed Infrared Bolometer," Rev. Sci. Instr., 33, 964-972 (1962), also Avco-Everett Research Laboratory Research Report 120, March 1962.

9. Camm, J. C. and Rose, P. H., "Electric Shock Tube for High Velocity Simulation," Phys. Fluids, 6, 663-678 (May 1963).

10. Carslaw, H. S. and Jaeger, J. C., Conduction of Heat in Solids, Oxford at the Clarendon Press, 1959, 2nd Edition, 55-75-76.

11. Feldman, S., "Hypersonic Gas Dynamic Charts for Equilibrium Air," Avco-Everett Research Laboratory Research Report 40, January 1957.

12. Kemp, N.H., "Approximate Analytical Solution of Similarity Boundary Layer Equations with Variable Fluid Properties," Fluid Mechanics Laboratory, Massachusetts Institute of Technology, Research Report to be published, 1964.

13. Rose, P.H. and Stark, W.I., "Stagnation Point Heat Transfer Measurements in Dissociated Air," J. Aerospace Sci., 25, 86-97 (1958).

14. Roshko, A., "On Flow Duration in Low Pressure Shock Tubes," Phys. Fluids, 3, 835-842 (1960).

15. Oppenheim, U.P. and Goldman, A., "Infrared Spectral Transmittance of MgO and BaF_2 Crystals between 27° and $1000^\circ C$," Jour. of the Optical Society of America, 54, 127-128 (Jan. 1964).

16. Garber, A.M., Nolan, E.J. and Scala, S.M., "Pyrolytic Graphite - A Status Report," General Electric-R-63SD84, October 1963.

17. Holland, L., Vacuum Deposition of Thin Films, John Wiley & Sons, 1960.

18. Hass, G., Edit., Physics of Thin Films, Vol. 1, Academic Press, 1963.

19. Camac, M. and Feinberg, R.M., "Thermal Conductivity of Argon at High Temperatures," Avco-Everett Research Laboratory Research Report 168, March 1963.

20. American Inst. of Physics Handbook, 2nd Edition, McGraw-Hill Co., New York, 1963.

21. Gubareff, C.G., et al, "Thermal Radiation Properties Survey," 2nd Edit., Honeywell Research Center, Minneapolis, Minn., 1960.

22. Beckman DK-2 Ratio Recording Spectrophotometer Instruction Manual, Beckman Instruments, Inc., 1962.

23. Edwards, D.K., et al, "Integrating Sphere for Imperfectly Diffuse Samples," J.O.S.A., 51, 1279.

24. Kivel, B. and Bailey, K., "Tables of Radiation from High Temperature Air," Avco-Everett Research Laboratory Research Report 21, December 1957.

25. Allen, R.A., "New Measurement and a New Interpretation for High Temperature Air Radiation," AIAA Preprint 64-72, (January 1964).

26. Wilson, J., "Ionization Rates of Air behind High Speed Shock Waves," Avco-Everett Research Laboratory Research Report (to be published).

27. Petschek, H. E. and Byron, S., "Approach to Equilibrium Ionization behind Strong Shock Waves in Argon," Annals of Physics, $\underline{1}$, 270-315, (1957).

28. Lin, S. C. and Teare, J. D., "Rate of Ionization behind Shock Waves in Air. II. Theoretical Interpretation," Phys. Fluids, $\underline{6}$, 355-374 (March 1963).